THE USE OF BOUNDARY-LAYER CONTROL TO ESTABLISH FREE STREAM-LINE FLOWS

By D. G. Hurley

Aeronautical Research Laboratories,
Department of Supply, Australia

1. INTRODUCTION

For more than ten years research on boundary layer control has been proceeding at the Aeronautical Research Laboratories.

The emphasis was originally on maintaining laminar flow on a thick Griffith type suction aerofoil and the work embraced wind-tunnel and flight testing. It was established that this type of aerofoil could be made airworthy and that its low drag characteristics could be achieved in flight. However, due to its large thickness/chord ratio the wing had a low critical Mach number and this limited its practical application so that further work on this line was abandoned.

Thus about seven years ago the emphasis shifted to using boundary layer control for increasing lift. This work has followed a number of lines. Mr. R. A. Wallis suggested air jets as a method of boundary layer control and has shown that they can be used to delay the onset of separation and also to reduce its adverse effects once it has occurred. This paper is concerned with a different attack on the problem.

Now for an aircraft to have good performance at supersonic speeds its wings must be thin and have highly curved or even sharp leading edges. If no special measures are taken the low speed performance of these wings will be poor* because the flow will separate from the leading edge for other than very small values of the lift coefficient. This separation leads to small values of maximum lift, large drags, poor controllability and also buffeting.

The conventional methods of improving the low speed performance of these wings consist of taking measures to reduce the adverse effects of these separations. Thus the leading edge of the wing may be drooped or it may be fitted with a leading edge slat to postpone the occurrence of separation to a larger incidence. It is also usual to employ a trailing edge flap on which boundary layer control may be used if increased flap effectiveness is required.

* A partial exception is the thin slender delta in which case all the effects of separation are not adverse. Remarks on the possible application of the scheme described in the paper to this wing are made on page 706.

The basic idea behind the work to be described was to devise a method of exploiting rather than suppressing this leading edge separation. It was felt that a possible method would be to permit the flow to separate from the leading edge and to use boundary layer control to make it reattach and remain attached to the upper surface of a forward facing flap which

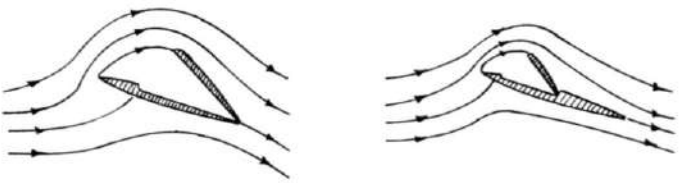

FIG. 1. Possible forms of free stream-line flap.

would be mounted above the wing as shown in Fig. 1. Thus a flow would be established about a very thick pseudo-wing which could be expected to have good low speed properties.

This paper describes a theoretical and experimental investigation of the potentialities of this scheme. The work so far has been confined to two-dimensional flows but some of the problems and possible benefits of three-dimensional effects will be indicated.

The experiments were carried out at A.R.L. between April 1957 and January 1958.

SYMBOLS

C_D	Form drag coefficient: $C_D = \dfrac{D}{\frac{1}{2}\rho U^2 l_2}$
C_{DT}	"Total" drag coefficient: $C_{DT} = C_D + C_\mu$
C_H	Total head coefficient
C_L	Lift coefficient: $C_L = \dfrac{L}{\frac{1}{2}\rho U^2 l_2}$
C_{LD}	Theoretical value of C_L when $\alpha = \alpha_D$
C_M	Pitching moment about quarter chord point of lower plate
C_p	Pressure coefficient
C_p^*	Pressure coefficient on free stream-line
$C_{p.\ T.E.}$	Pressure coefficient on outer surface of upper plate at 0·4 in. upstream of trailing edge
C_μ	Momentum coefficient
$C_{\mu\text{crit}}$	See p. 691
$C_{\mu R}$	See p. 704
d	Parameter. See Fig. 4
d'	Slot width
f	Parameter. See equation (7)
K	Circulation

L	Length of free stream-line
l_1	Length of flat portion of upper surface of flap and of upper plate of theoretical solution
l_2	Length of lower plate
N	Frequency
Q	See equation (1)
q	Fluid speed
q_l	Maximum value of q on portion AD_2 of aerofoil when $\alpha = \alpha_D$, see Fig. 2
q_m	Theoretical value of q on free stream-line when $\alpha = \alpha_D$
u	Velocity in boundary layer and in mixing region, see Figs. 13 and 35
U	Free stream velocity
U^*	Velocity at outer edge of mixing region
V_j	Slot velocity
w	$w = \phi + i\psi$
x, y	$z = x + iy$
x_1	Distance along upper plate from front of flat portion
x_2	Distance along lower plate from leading edge
y'	See Fig. 13
z	Physical plane, see Fig. 2
z_1, z_2	See Fig. 5 and equation (13)
α	Incidence of lower plate
α_{crit}	See p. 691
α_D	Value of α for which potential solution exists
β	See Fig. 5
γ	Slot angle, see Fig. 10
δ	Boundary layer thickness
ζ	$\zeta = \xi + i\eta$, see Fig. 4
ζ_1	Value of ζ corresponding to point at infinity in z-plane
θ	Direction of flow, see equation (1), and momentum thickness of boundary layer
θ_R θ'_R	See p. 703
ρ	Air density
τ	Trailing edge angle

2. POTENTIAL THEORY

Problem Considered

It was felt that the initial two-dimensional experiments should be carried out on a wing-flap arrangement that was simple enough to enable calculations of the potential flow to be made. The arrangement that was chosen for the calculations[1] is shown in Fig. 2. It consists of two flat plates of lengths l_1 and l_2 which are hinged together at their rear at an angle τ, the lower one being at an incidence, α_D, to a uniform stream of speed U.

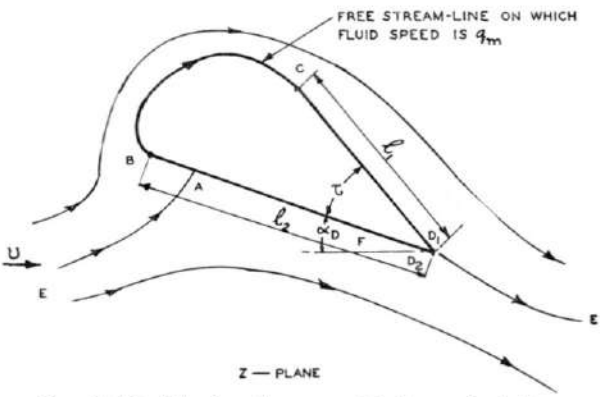

FIG. 2. Model taken for potential flow calculations.

If the flow were to separate from the leading edge of the lower plate and to reattach to the leading edge of the upper plate (as is desired) then it is to be expected that the pressure (and thus the fluid speed) would be nearly constant along a stream-line which would join the leading edges of the two plates. Thus solutions to the potential flow about a pseudo-body consisting of the two flat plates joined by a free stream-line on which the fluid speed is q_m are sought. The free stream-line must meet each of the plates tangentially, as shown in the figure, as otherwise there would be an infinite velocity at the junction. It is assumed that the circulation is fixed by the Kutta–Joukowski condition being satisfied at the trailing edge of the combination.

Determination of $\mathrm{d}w/\mathrm{d}z$ *as a function of* ζ

Figure 3 shows the trace of the "aerofoil" in the Q-plane where

$$\left.\begin{aligned} Q &= \log\left(-U\frac{\mathrm{d}z}{\mathrm{d}w}\right) \\ &= \log\frac{U}{q} + i\theta \end{aligned}\right\} \qquad (1)$$

Here $w = \phi + i\psi$ is the complex velocity potential, q the fluid speed and θ the direction of flow. The velocity components u and v are given by

$$u = -\frac{\partial\phi}{\partial x} \qquad v = -\frac{\partial\phi}{\partial y} \qquad (2)$$

Points in the z and Q planes which correspond are designated by the same letter. Since the trailing edge angle of the aerofoil is not zero there will be a stagnation point there so that the points D_1 and D_2 on either side of it will map to $Q = +\infty - i(\alpha_D + \tau)$ and $Q = +\infty - i\alpha_D$ respectively. Since q is zero at A and at the trailing edge it will have a local maximum, q_t, at some point F, between A and the trailing edge. The point

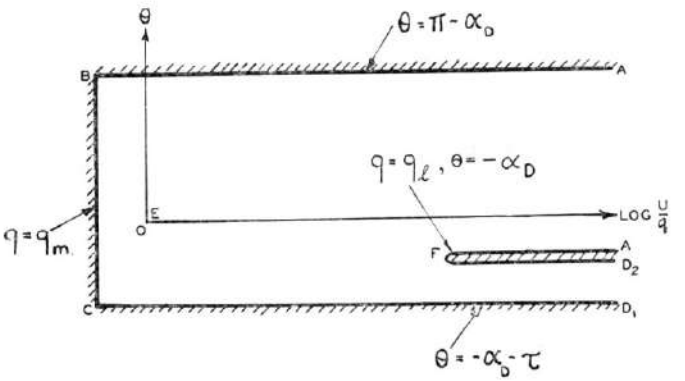

FIG. 3. Q-plane.

at infinity in the z-plane maps to the origin of the Q-plane and the region exterior to the aerofoil maps to the unhatched region of the Q-plane.

The Schwartz–Christoffel transformation is used to map the unhatched portion of the Q-plane on to the upper half of the ζ-plane (Fig. 4) and this gives

$$\frac{dQ}{d\zeta} = K1\,(\zeta + 1)^{-\frac{1}{2}}\,(\zeta - 1)^{-\frac{1}{2}}\,(\zeta - d)^{-1}\,(\zeta - f) \tag{3}$$

where the points A, B, and C of the Q-plane have been mapped to $\zeta = \infty$, -1 and $+1$ respectively and K_1 is a constant. The points to which D, E, and F map are designated by $\zeta = d$, ζ_1, and f respectively.

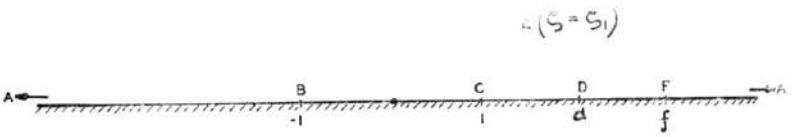

FIG. 4. ζ-plane

Equation (3) may be integrated to give

$$Q = K_1 \log\left[\zeta \pm (\zeta^2 - 1)^{1/2}\right] + \frac{K_1(d - f)}{(d^2 - 1)^{1/2}} \log\left[\frac{1}{\zeta - d}\left(1 - d\zeta \pm (d^2 - 1)^{1/2}\,(\zeta^2 - 1)^{1/2}\right)\right] + K_2 \tag{4}$$

where K_2 is an arbitrary constant.

In equation (4) the positive sign is taken in each place where there is an alternative, $(\zeta^2 - 1)^{1/2}$ is taken to behave as ζ for ζ large and each of the logarithms is taken to have its principle value. With these determinations

it can be shown that the point-to-point correspondences between the Q and ζ-planes shown in Figs. 3 and 4 are satisfied if

$$K_1 = 1 \tag{5}$$

$$K_2 = \log \frac{U}{q_m} - i(\alpha_D + \tau) \tag{6}$$

$$\frac{d - f}{(d^2 - 1)^{1/2}} = -\frac{\tau}{\pi} \tag{7}$$

$$\log \frac{q_m}{q_z} = \log[f + (f^2 - 1)^{1/2}] - \frac{\tau}{\pi} \log \left\{ \frac{1}{f - d} [df - 1 - (d^2 - 1)^{1/2} (f^2 - 1)^{1/2}] \right\} \tag{8}$$

and

$$\frac{q_m}{U} \exp i(\alpha_D + \tau) = \frac{\zeta_1 + (\zeta_1^2 - 1)^{1/2}}{\left\{ \frac{1}{\zeta_1 - d} - d [1 - d\zeta_1 + (d^2 - 1)^{1/2} (\zeta_1^2 - 1)^{1/2}] \right\}^{\tau/\pi}} \tag{9}$$

From equations (1), (4), (5), (6), and (7) it follows that

$$\frac{dz}{dw} = -\frac{[\exp -i(\alpha_D + \tau)]\{\zeta + (\zeta^2 - 1)^{1/2}\}}{q_m \left\{ \frac{1}{\zeta - d} [1 - d\zeta + (d^2 - 1)^{1/2} (\zeta^2 - 1)^{1/2})] \right\}^{\tau/\pi}} \tag{10}$$

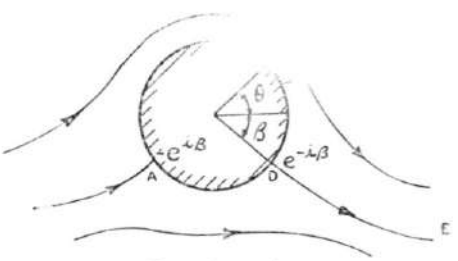

FIG. 5. Z_1-plane

Determination of $dw/d\zeta$

Figure 5 shows the result of mapping the exterior of the aerofoil in the z-plane on to the exterior of the unit circle in the z_1-plane, the mapping being the one which leaves the region at infinity unaltered (i.e. the one for which $dz/dz_1 \to 1$ as $z \to \infty$). Thus the stagnation points at A and D will be symmetrically located in the z_1-plane as shown and the complex velocity potential will be

$$w(z_1) = -Uz_1 - \frac{U}{z_1} - \frac{iK}{2\pi} \log z_1 \tag{11}$$

where K is the circulation and is given by

$$K = 4\pi U \sin \beta \tag{12}$$

The exterior of the unit circle in the z_1-plane is mapped on to the interior of the unit circle in the z_2-plane by the transformation

$$z_1 = \frac{1}{z_2} \tag{13}$$

and then on to the upper half of the ζ-plane by the transformation

$$z_2 = \lambda \frac{\zeta - \zeta_1}{\zeta - \bar{\zeta}_1} \tag{14}$$

where $|\lambda| = 1$.

The transformation (14) ensures that the point $\zeta = \zeta_1$ maps to the origin of the z_2-plane and thus by equation (13) to the point at infinity in the z_1 and z-planes as required.

Elimination of z_2 between equations (13) and (14) yields

$$z_1 = \frac{1}{\lambda} \frac{\zeta - \bar{\zeta}_1}{\zeta - \zeta_1} \tag{15}$$

The stagnation points at $z_1 = -e^{i\beta}$ and at $z_1 = e^{-i\beta}$ must map to $\zeta = \infty$ and $\zeta = d$ respectively so that from equation (15)

$$\lambda = -e^{-i\beta} \tag{16}$$

and

$$d = \xi_1 + \eta_1 \tan \beta \tag{17}$$

where $\zeta_1 = \xi_1 + i\eta_1$

From equations (11), (15), and (16) it follows that

$$w(\zeta) = Ue^{i\beta} \frac{\zeta - \bar{\zeta}_1}{\zeta - \zeta_1} + Ue^{-i\beta} \frac{\zeta - \zeta_1}{\zeta - \bar{\zeta}_1} - \frac{iK}{2\pi} \log\left| - e^{-i\beta} \frac{\zeta - \bar{\zeta}_1}{\zeta - \zeta_1}\right| \tag{18}$$

Differentiation of this equation gives

$$\frac{dw}{d\zeta} = -\frac{2iU\eta_1 e^{i\beta}}{(\zeta - \zeta_1)^2} + \frac{2iU\eta_1 e^{-i\beta}}{(\zeta - \bar{\zeta}_1)^2} - \frac{iK}{2\pi}\left(\frac{1}{\zeta - \bar{\zeta}_1} - \frac{1}{\zeta - \zeta_1}\right) \tag{19}$$

Substituting for K from equation (12) yields, after some simplification,

$$\frac{dw}{d\zeta} = -\frac{8U\eta_1^2(d - \xi)\cos\beta}{[(\xi - \xi_1)^2 + \eta_1^2]^2} \tag{20}$$

for $\zeta = \xi$, i.e. for ζ on the real axis.

Closure Condition

The shape of the "aerofoil" is obtained from

$$z = \int \frac{dz}{d\zeta} d\zeta = \int \frac{dz}{dw} \frac{dw}{d\zeta} d\zeta \tag{21}$$

where dz/dw and $dw/d\zeta$ are given by equations (10) and (20), the integration being carried out along the real ζ-axis.

Now equations (10) and (19) show that for ζ large

$$\frac{dz}{d\zeta} \sim \frac{K_3}{\zeta^2}$$

where K_3 is a constant, so that the condition that the aerofoil should close up may be written

$$\oint_{\mathscr{C}} \frac{dz}{d\zeta} d\zeta = 0$$

where the path of integration $\mathscr{C}$ is the real axis, indented above $\zeta = \pm 1$ and d, and a large semi-circle lying in the upper half of the ζ-plane.

The only singularity of $dz/d\zeta$ within $\mathscr{C}$ is at $\zeta = \zeta_1$ so that the closure condition is that the residue of $dz/d\zeta$ at $\zeta = \zeta_1$ should be zero. It can be shown from equations (10) and (19) that this gives

$$\frac{1}{(\zeta_1^2 - 1)^{1/2} - (\zeta_1 - d)(\zeta_1^2 - 1)^{1/2}} \frac{\frac{\tau}{\pi}(d^2 - 1)^{1/2}}{} = \frac{-i(\xi_1 - d)}{\eta_1(\zeta_1 - d)} \tag{22}$$

Calculation Procedure

The shape of a particular "aerofoil" is calculated from equation (21) using the values of dz/dw and $dw/d\zeta$ given by equations (10) and (20).

However, before this is done a set of parameters must be obtained which satisfies equations (7), (8), (9), (17), and (22). Two of these equations, (9) and (22), are complex so that there are 7 relationships that must be satisfied by the 9 parameters, f, q_l/U, q_m/U, ξ_1, η_1, d, τ, α_D, and β. Thus the family of solutions will be a two-parameter one.

It can be shown that equation (22) has one and only one acceptable root for $\zeta_1 = \xi_1 + i\eta_1$ which is given by

$$\xi_1 = \frac{-fd^2 + f^3 + 2f - f(f-d)\{(d+f)^2 - 4\}^{1/2}}{2(2f^2 + 1 - 2df)} \tag{23}$$

$$\eta_1 = \frac{\xi_1^{1/2}(d - \xi_1)}{(f - \xi_1)^{1/2}} \tag{24}$$

where $f = d + \frac{\tau}{\pi}(d^2 - 1)^{1/2}$

To satisfy the various relationships the following procedure is followed

(i) d, which must lie in the range $(1, \infty)$ (see Fig. 4) and τ are selected,
(ii) Equation (23) is solved for ξ_1,
(iii) Equation (24) is solved for η_1,
(iv) Equation (9) is solved for q_m/U and α_D,
(v) Equations (17), (7), and (8) are solved in turn for β, f, and q_l respectively.

When a consistent set of parameters has been found in this way, the shape of the aerofoil may be calculated from equation (21) and the velocities on its surface from equation (10).

Results and Discussions

The calculation procedure described above was carried out for various values of τ and d and results are given in Table 1 and Fig. 6. The figure

TABLE 1

Main features and parameter values of various aerofoils

τ°	d	q_m	α°_D	l_1	l_2	l_1/l_2	ξ_1	η_1	β°	C_{LD}
10	1·0	1·000	0	0	4·00	0	1·0000	0	0	0
	1·1	1·711	7·28	2·32	3·59	0·645	1·0814	0·0922	11·41	1·38
	1·3	2·292	13·18	2·72	3·49	0·778	1·2226	0·2434	17·63	2·18
	1·6	2·941	19·65	3·00	3·48	0·862	1·3875	0·4714	24·26	2·97
	2·0	3·625	26·26	3·00	3·39	0·886	1·5383	0·7666	31·06	3·82
	5·0	5·792	54·10	3·24	3·39	0·957	1·3988	2·1641	59·00	6·35
	∞	6·727	85·00	3·34	3·34	1·000	0	2·9594	90·00	7·52
30	1·0	1·000	0	0	4·00	0	1·0000	0	0	0
	1·1	1·891	8·87	1·32	3·38	0·392	1·0425	0·1605	19·72	2·51
	1·3	2·442	17·20	1·68	3·16	0·531	1·0905	0·3709	29·46	3·91
	1·6	2·953	25·66	1·96	3·01	0·649	1·1012	0·6225	38·70	5·22
	2·0	3·382	33·67	2·11	2·93	0·722	1·0563	0·8737	47·20	6·29
	5·0	4·248	56·86	2·29	2·73	0·839	0·5962	1·4883	71·33	8·72
	∞	4·464	75·00	2·60	2·60	1·000	0	1·6638	90·00	9·67
60	1·0	1·000	0	0	4·00	0	1·0000	0	0	0
	1·1	2·058	7·79	0·61	3·12	0·197	0·9831	0·2233	27·64	3·76
	1·3	2·558	16·92	1·02	2·80	0·363	0·9361	0·4399	39·60	5·72
	1·6	2·925	24·88	1·28	2·60	0·493	0·8472	0·6408	49·59	7·36
	2·0	3·180	31·70	1·47	2·47	0·594	0·7343	0·7989	57·74	8·60
	5·0	3·579	48·49	1·81	2·18	0·829	0·3341	1·0745	77·03	11·23
	∞	3·659	60·00	2·00	2·00	1·000	0	1·1340	90·00	12·67
90	1·0	1·000	0	0	4·00	0	1·0000	0	0	0
	1·1	2·196	7·01	0·42	2·95	0·144	0·9254	0·2643	33·44	4·69
	1·3	2·621	14·07	0·75	2·59	0·288	0·8189	0·4598	46·30	7·01
	1·6	2·895	20·38	0·98	2·36	0·413	0·6925	0·6101	56·08	8·85
	2·0	3·065	25·51	1·14	2·21	0·517	0·5700	0·7125	63·51	10·18
	5·0	3·301	37·30	1·47	1·87	0·786	0·2380	0·8651	79·70	13·22
	∞	3·342	45·00	1·68	1·68	1·000	0	0·8944	90·00	14·96
120	1·0	1·000	0	0	4·00	0	1·0000	0	0	0
	1·1	2·290	5·00	0·34	2·87	0·117	0·8712	0·2921	38·06	5·40
	1·3	2·659	10·00	0·62	2·47	0·252	0·7274	0·4601	51·21	7·93
	1·6	2·870	14·30	0·83	2·22	0·371	0·5880	0·5714	60·55	9·86
	2·0	2·992	17·69	0·98	2·04	0·481	0·4695	0·6400	67·31	11·37
	5·0	3·148	25·20	1·33	1·70	0·781	0·1875	0·7332	81·34	14·61
	∞	3·175	30·00	1·50	1·50	1·000	0	0·7499	90·00	16·76
150	1·0	1·000	0	0	4·00	0	1·0000	0	0	0
	1·1	2·361	2·64	0·30	2·82	0·108	0·8211	0·3109	41·89	5·95
	1·3	2·682	5·23	0·58	2·40	0·240	0·6544	0·4515	55·03	8·58
	1·6	2·850	7·40	0·77	2·15	0·356	0·5125	0·5336	63·86	10·49
	2·0	2·941	9·07	0·98	1·98	0·495	0·4012	0·5806	70·04	11·93
	5·0	3·052	12·71	1·25	1·62	0·767	0·1561	0·6405	82·47	15·38
	∞	3·083	15·00	1·42	1·42	1·000	0	0·6507	90·00	17·70
180	1·0	1·000	0	0	†	0	1·0000	0	0	0
	1·1	2·418	0	†	†	†	0·7753	0·3231	45·14	†
	1·3	2·698	0	†	†	†	0·5947	0·4389	58·11	†
	1·6	2·833	0	†	†	†	0·4551	0·4992	66·44	†
	2·0	2·904	0	†	†	†	0·3515	0·5316	72·13	†
	5·0	2·987	0	†	†	†	0·1344	0·5708	83·31	†
	∞	3·000	0	†	†	1·000	0	0·5773	90·00	†

† Not calculated

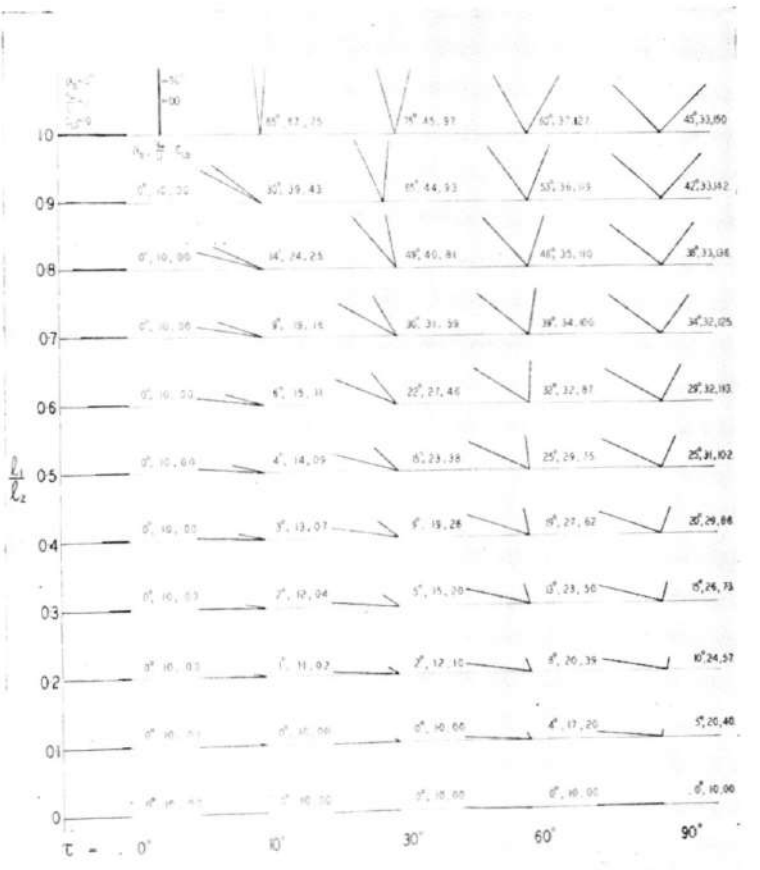

FIG. 6. Family of "aerofoils".

shows that for a given relative geometry of the plates (given values of l_1/l_2 and τ) there is a solution for only one particular value of α_D. Surprisingly large values of C_L are seen to be attained although the larger ones involve quite impractical plate configurations.

Values of 0·6 and 30° for z_1/z_2 and τ respectively, were selected for the main series of experiments described below and then

$$\alpha_D = 21{\cdot}8°$$
$$q_m/U = 2{\cdot}73$$

and

$$C_{LD} = 4{\cdot}63$$

Figure 7 gives the shape of the "aerofoil" and Fig. 8, the velocities on the plates.

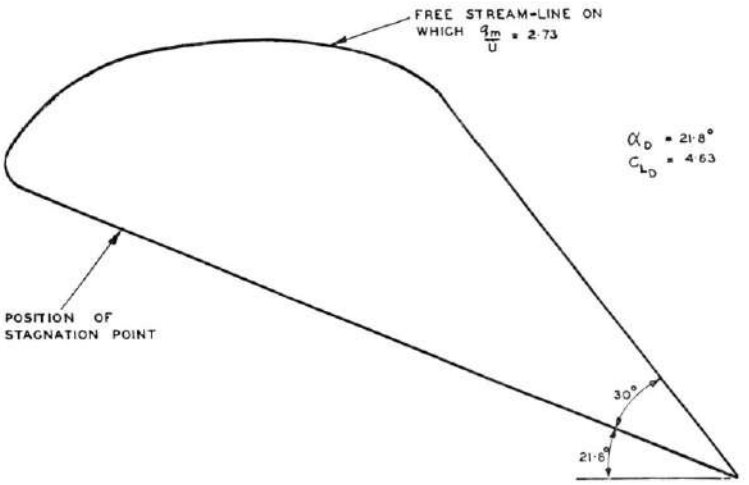

FIG. 7. Potential solution when $l_1/l_2 = 0{\cdot}6$ and $\tau = 30°$.

A smaller number of experiments were also carried out with $l_1/l_2 = 0{\cdot}6$ and $\tau = 45°$, when

$$\alpha_D = 29°$$

$$q_m/U = 3{\cdot}1$$

and

$$C_{LD} = 6{\cdot}9$$

3. DESIGN OF EXPERIMENTS

The primary purpose of the experiments[2] was to find out if it were possible to establish flows which resembled the potential solutions and thus to realise the large lift coefficients predicted by the theory. The main experiments referred to the case when $l_1/l_2 = 0{\cdot}6$ and $\tau = 30°$. Figure 8 shows that there are large adverse velocity gradients on the upper plate so that for the experiments to succeed some form of boundary layer control must be applied there to prevent separation. It was felt that the most likely way of establishing the desired flow would be to fit the upper plate with a rounded leading edge and to incorporate in this leading edge a single blowing slot. The high velocity air discharged by the slot would then encourage the flow to reattach to the leading edge of the upper plate in virtue of its entrainment effect and at the same time it would prevent the flow from separating from the upper plate.

4. DESCRIPTION OF MODEL

The model was designed to enable two-dimensional pressure plotting tests to be carried out in the 36 in. by 20 in. low speed wind tunnel at the A.R.L. and is shown in Figs. 9 to 11. It consists of two 0·128 in. thick

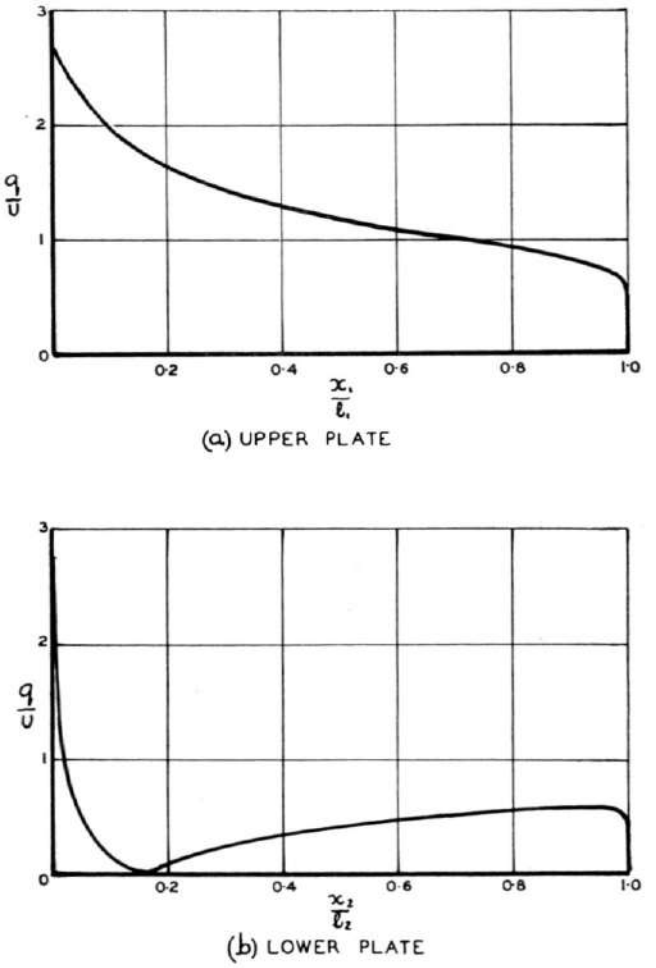

FIG. 8. The velocities on the plates when $l_1/l_2 = 0{\cdot}6$ and $\tau = 30°$.

brass plates of approximately 20 in. span, the upper plate is 5·4 in. long and the lower one 9·0 in. long giving the required value of 0·6 for l_1/l_2 (see p. 671). The front of the lower plate was bevelled at 45° so forming a sharp leading edge. The two plates were hinged along the 20 in. dimension so that τ could be changed, the hinge being sealed to prevent leakage.

Circular end plates of thin brass were attached and sealed to either end of the model and rotated with it during change of incidence.

A brass tube having an outside diameter of 0·875 in. and incorporating a 0·006 in. wide blowing slot was mounted at the leading edge of the upper plate. The mounting of the tube was such that the angle between the upper plate and the slot exit, the angle designated by γ in Fig. 10, could be changed keeping the upper plate tangential to the tube.

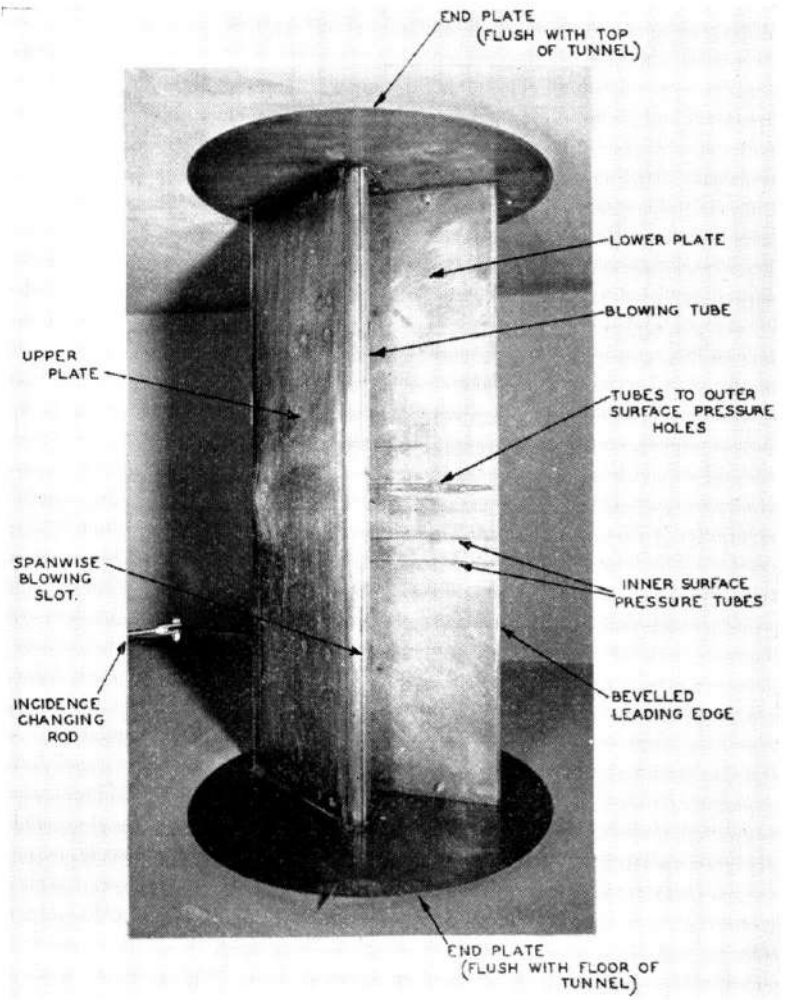

FIG. 9. View of model in tunnel.

The model was provided with flush static pressure holes near the mid-span section on the outer surfaces of the plates and around the blowing tube. On the inner surfaces of the plates this technique was not practicable and creepers were used instead. The chordwise locations of the pressure holes are given in Figs. 10 and 11.

The mass flow and the total pressure of the air discharged by the slot were measured and used to calculate the value of C_μ, the momentum coefficient of the air discharged by the slot.

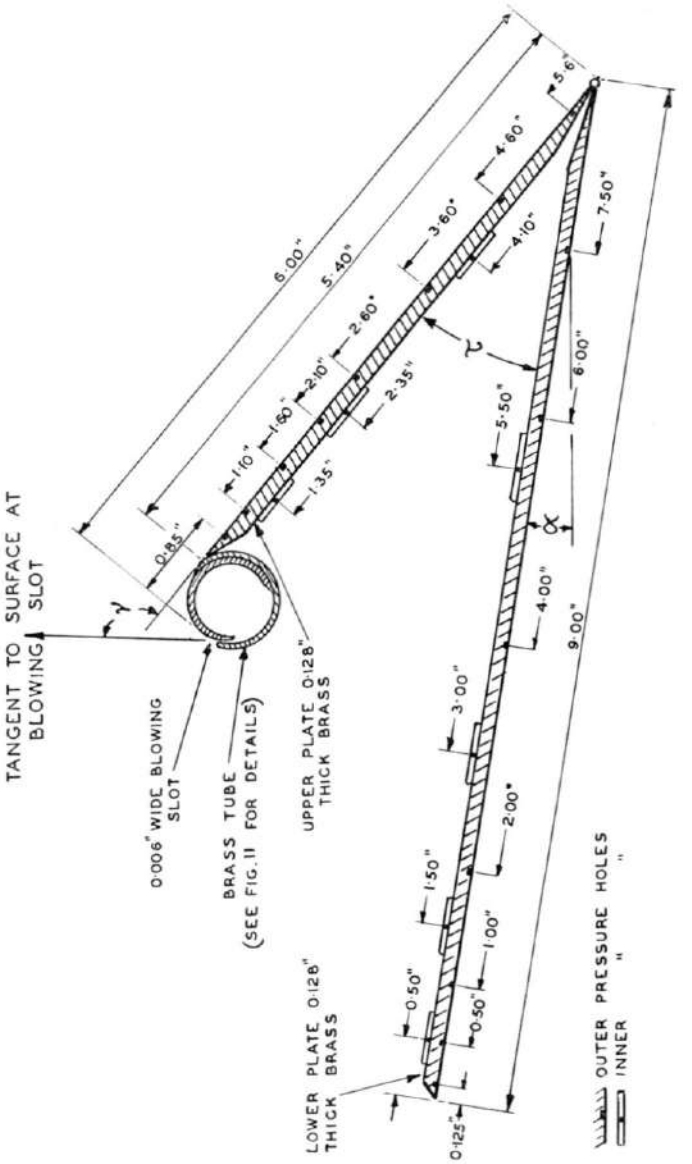

FIG. 10. Model dimensions.

5. TESTS CARRIED OUT

In the first series of tests τ was 30° and γ, 130°†. Pressure distributions were measured for various values of α and C_μ for a wind speed of 50 ft/sec,

† Preliminary bench tests showed that the Coanda effect caused the high-velocity air discharged by the slot to adhere to the upper surface of the upper plate provided that γ was not greater than about 130°.

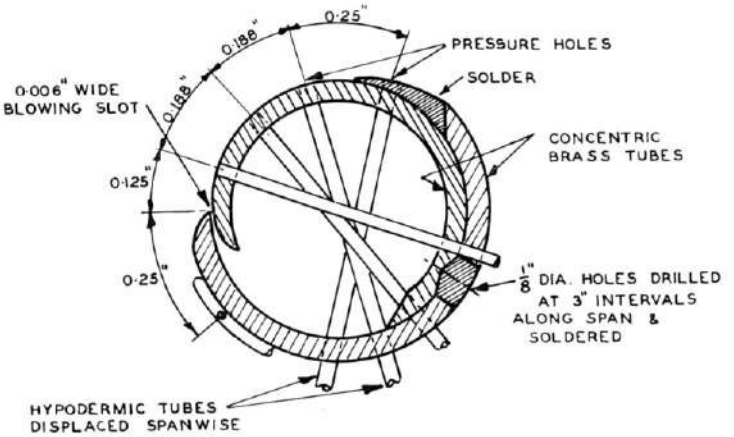

FIG. 11. Blowing tube and slot construction.

giving a Reynolds number based on l_2 of $2{\cdot}43 \times 10^5$. α was increased from zero to the test value with $C_\mu = 0$ and then C_μ was increased through the test values. Checks showed that the same pressure distributions were obtained when C_μ was decreased through the test values which indicates that hysteresis effects are small. Investigations of the mixing region, which replaces the free stream-line envisaged by the theory, were carried out using total head and static pressure probes.

During the tests it was observed that a regular audio note was emitted by the model and its frequency and relative amplitude were measured.

A smaller number of tests was also carried out for the following cases

$$(1)\ \gamma = 130^\circ \qquad \tau = 45^\circ$$

$$(2)\ \gamma = 90^\circ \qquad \tau = 30^\circ$$

A liquid film technique similar to that reported in Ref. 3 was used to investigate the flow near the leading edge of the upper plate. A thin brass plate fitting very closely around the blowing tube, was rigidly attached to the model at right angles to the axis of the tube. This plate was covered with a piece of black paper which was coated with a suspension of titanium oxide in oleic acid diluted with a small amount of kerosene. The tunnel was started and then the blowing air was turned on. The consistency of the fluid coating was such that it only started to flow after the blowing had been turned on. When the pattern had developed the piece of paper was removed and renewed. The pressure distributions were noted whilst the flow visualization work was being carried out and it was found that they agreed well with those that were measured during the pressure plotting work. This shows that the flow visualization technique that was used does not unduly disturb the flow.

6. REDUCTION OF EXPERIMENTAL RESULTS AND THEIR ACCURACY

The lift, drag, and pitching moment acting on the model were obtained from the measured pressures by appropriate integrations and resolutions. The force acting on the inner surface of the tube was included. Since the momentum of the air entering the tube is in the spanwise direction it can be assumed that this force is of magnitude C_μ and acts in the direction opposite to the slot exit.

Punched card equipment was used to reduce the pressures to coefficient form and then to integrate them by means of the trapezoidal rule for the forces and moment.

It is believed that the greatest source of error in the results is that which arises from using the trapezoidal rule for carrying out the integrations. These errors were investigated in eight cases by also performing the integrations by the square counting method. It was found that the values of C_L and C_D given by the trapezoidal rule were too high by averages of 0·06 and 0·10 respectively. It is therefore believed that the error in the C_L values is less than 2%. The percentage error in the C_D values is considerably larger but the values given are believed to be conservative, i.e. the true values are less than those given.

7. RESULTS AND DISCUSSION

$\tau = 30°$, $\alpha = 22°$, *and* $\gamma = 130°$

When $\tau = 30°$ the value of α for which a theoretical solution of the potential flow exists is 22° and the results obtained for this case with $\gamma = 130°$ will be considered first.

Pressure Distributions and Tuft Investigations. Figures 12(a), (b), and (c) give the pressure distributions and it is seen that for each value of C_μ the pressures on the inner surfaces of the two plates are nearly uniform and that as C_μ is increased the pressures become more negative. For $C_\mu = 0{\cdot}37$ the pressures are approximately equal to the theoretical value of the pressure along the free stream-line.

Investigations using a tufted rod showed that for each value of C_μ the flow separated from the leading edge of the lower plate and reattached to the front of the tube. For low values of C_μ separation took place once again only a short distance down-stream of the reattachment point. As C_μ was increased this point of separation moved down the outer surface of the upper plate until for $C_\mu = 0{\cdot}37$ the flow was completely attached to this surface. The pressures measured on the outer surface of the upper plate (Fig. 12(b)) confirm this behaviour. For $C_\mu = 0$ the pressure is nearly uniform for $x_1 > -0{\cdot}3$ in. showing that separation occurs near this value of x_1. As C_μ is increased the point downstream of which the pressure is nearly uniform approaches the trailing edge. For $C_\mu \geqslant 0{\cdot}37$ the pressure

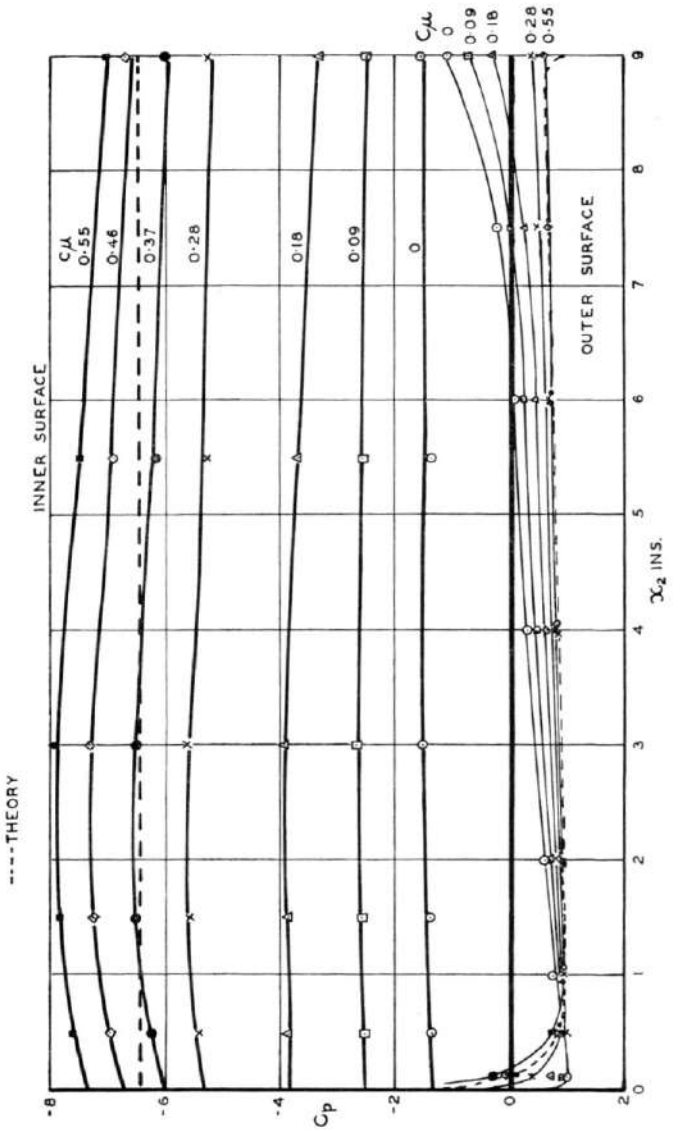

FIG. 12(a). Pressure distributions on lower plate for $\alpha = 22°$, $\gamma = 130°$, and $\tau = 30°$.

distributions are similar and resemble the theoretical curve with the exception of the pressures measured on the tube (i.e. when x_1 is negative) which are not included in the theory.

The tuft observations also showed that, except for the smallest values of C_μ, the flow left the leading edge of the lower plate in the direction of the tangent to the lower surface, as envisaged by the theory. The flow

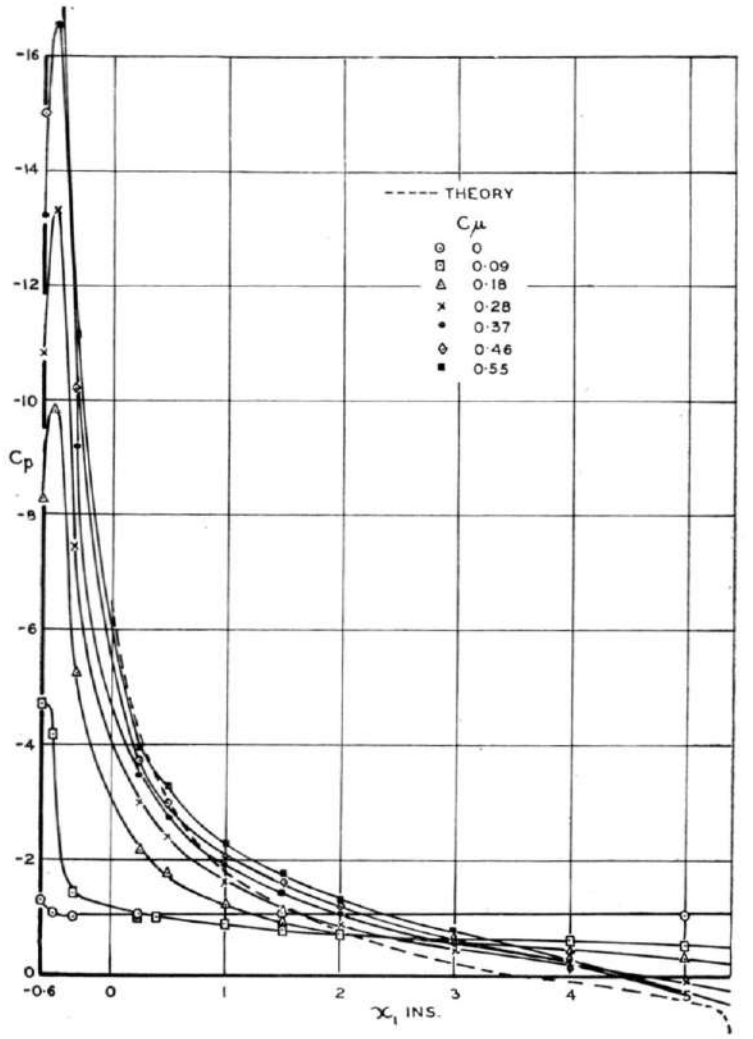

FIG. 12(b). Pressure distributions on outer surface of upper plate for $\alpha = 22°$, $\gamma = 130°$, and $\tau = 30°$.

outside a certain line joining the leading edge of the lower plate to the tube appeared to be perfectly steady. Inside this line the flow was turbulent and it was observed that the velocity decreased to low values at a short distance inside this line. In the region between the plates a fairly slow circulatory motion was detected. As C_μ was increased the line previously referred to became progressively more convex, a behaviour which is consistent with the pressures between the plates becoming more negative, as was observed (see Figs. 12(a) and (c)).

The flow visualization studies are discussed on p. 687.

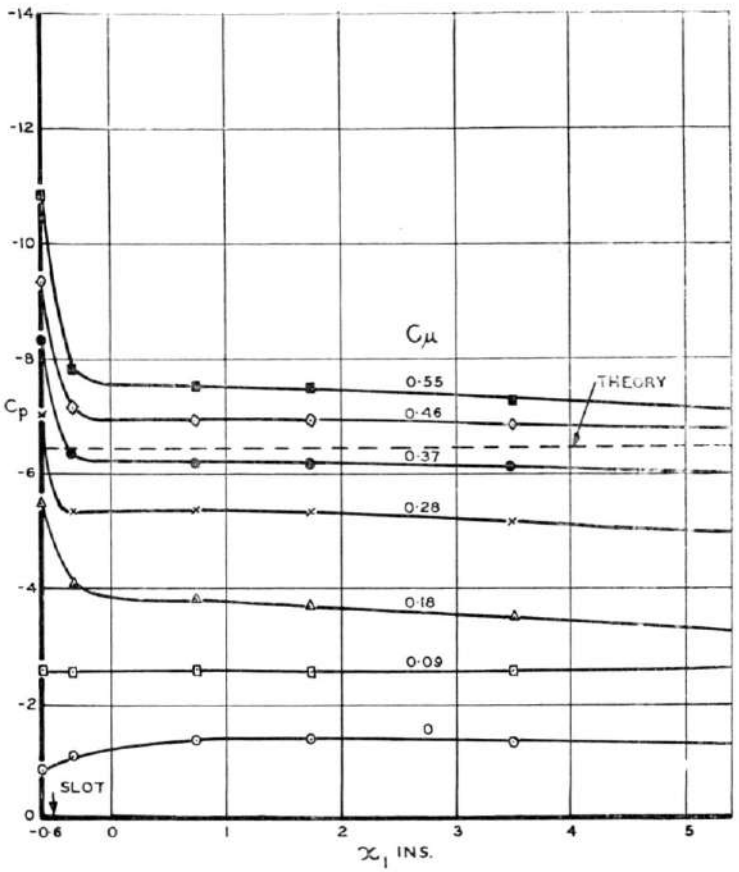

FIG. 12(c). Pressure distributions on inner surface of upper plate for $\alpha = 22°$, $\gamma = 130°$ and $\tau = 30°$.

Investigation of Mixing Region and Comparison with Mixing Length Theory. For $C_\mu = 0{\cdot}46$ a value slightly above that needed for complete flow attachment on the upper plate a total head and static pressure traverse was made across the turbulent mixing region along the line marked as the y' axis in Fig. 13. The hypodermic measuring tubes were aligned at 64° to this axis so as to lie approximately in the direction of the flow. The results of the traverses are given in Fig. 14 and the values of $[u/U]^2$ deduced therefrom are shown in Fig. 15. These latter results are shown in Fig. 13 and it is seen that the mixing region lies close to the position of the free stream-line of the potential theory.

Now the thickness of the boundary layer at the leading edge of the lower plate where the mixing region starts will be very small and also the pressure will be approximately constant along the mixing region. It is therefore reasonable to expect that the mixing region at a distance s along the

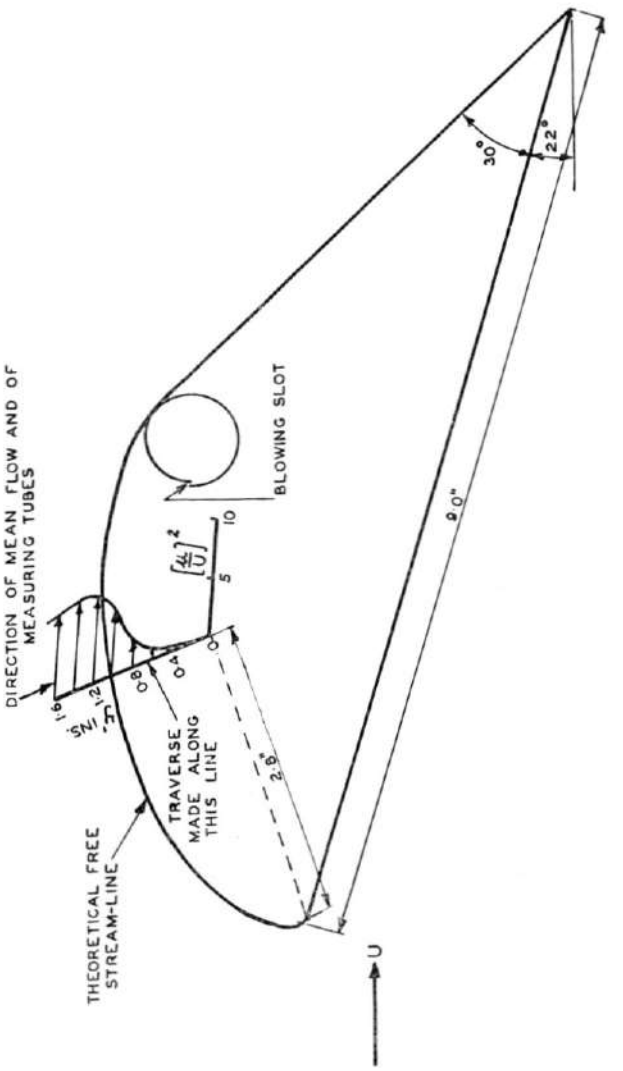

FIG. 13. Diagram showing mixing region and its position relative to theoretical free stream-line, $\alpha = 22°$, $C_\mu = 0{\cdot}46$, $\gamma = 130°$, and $\tau = 30°$.

theoretical free stream-line will resemble the mixing region at a distance s down-stream of the junction of a uniform stream with air at rest, the velocity of the uniform stream being U^*, the measured value of the velocity just outside the mixing region under investigation. This analogy is shown in Fig. 16.

The mixing of a uniform stream with air at rest has been treated by Tollmien using mixing length methods.[4] The velocity profile given by

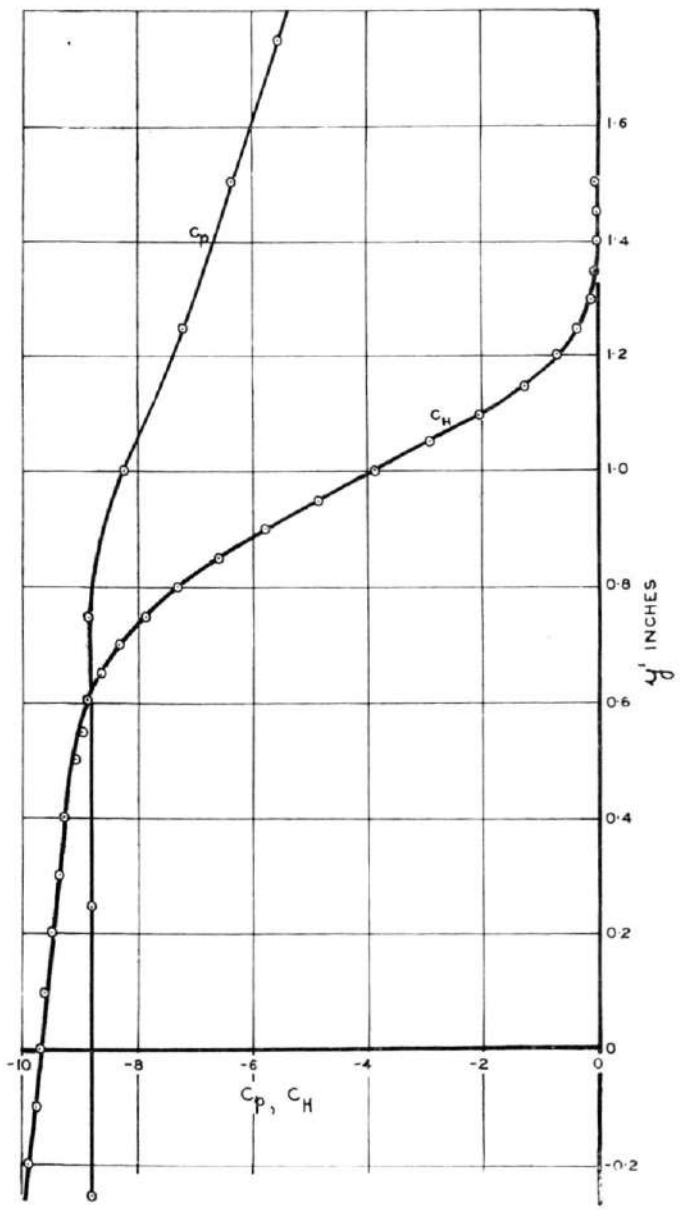

FIG. 14. Results of total head and static pressure traverses through mixing region.

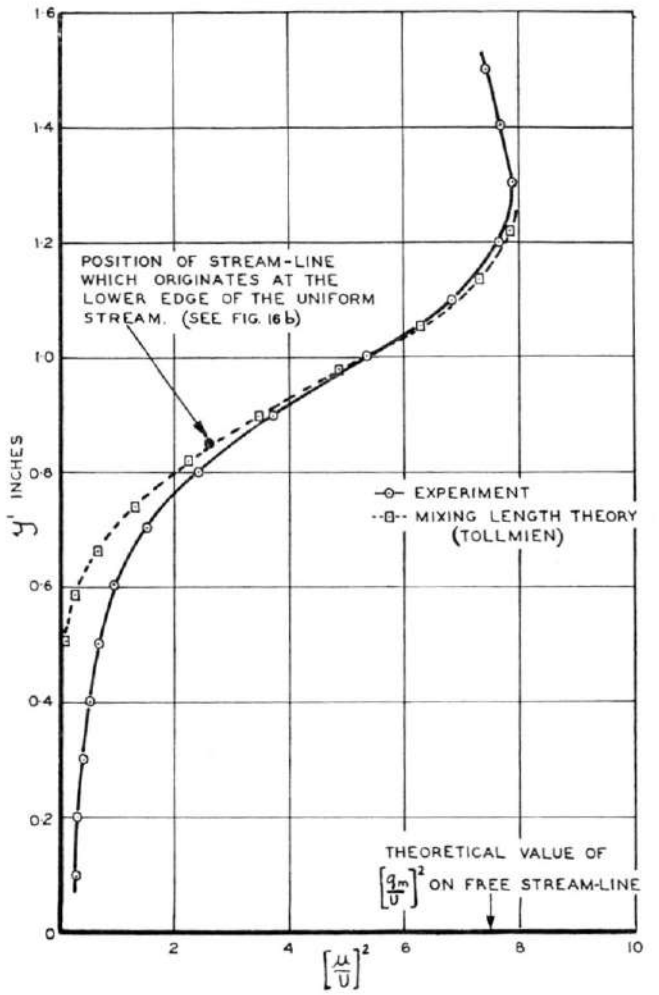

FIG. 15. Values of mean speed in mixing region and comparison with mixing length theory.

this method is compared with the experimental profile in Fig. 15. Included in the figure is the position, relative to the theoretical profile, of the stream-line which originates at the lower edge of the uniform stream (see Fig. 16). It is seen that outside this stream-line the theoretical and experimental curves agree quite well. Inside it the agreement is not so close. This is probably because the air which separates from the leading edge of the lower plate does not mix with air at rest but with air which is moving in the same direction at a small speed.

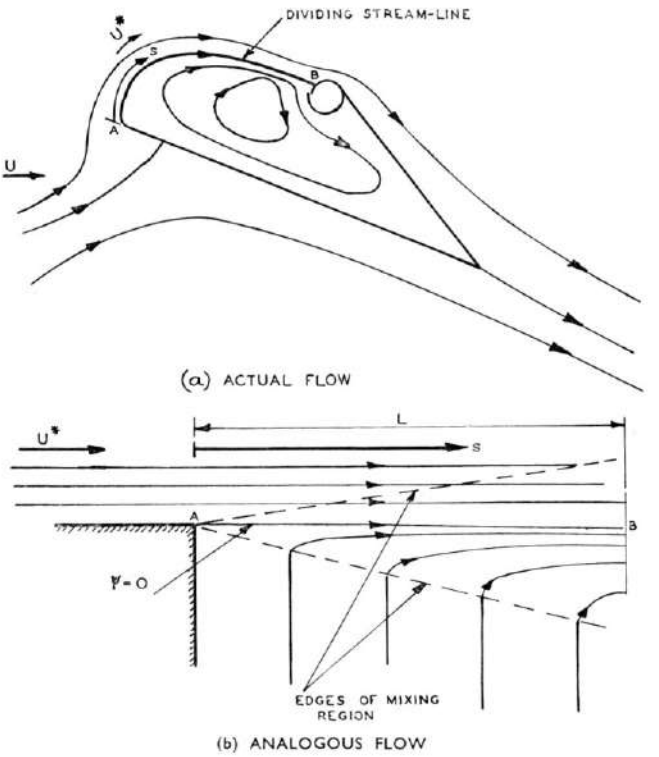

FIG. 16. Analogy between the mixing region and the mixing of a uniform stream with air at rest.

The agreement between the experimental velocity profile and the predictions of mixing length theory noted above was considered to be sufficiently close to justify extending the theory to give an estimate of the value of C_μ that is needed to establish the free stream-line type flow. As this extension applies to general values of α it is deferred until § 8.

$\tau = 30°$, $\gamma = 130°$, and Various Values of α

The results obtained for general values of α will now be considered.

Pressure Distributions. The pressure distributions for $C_\mu = 0{\cdot}46$ and various values of α are shown in Figs. 17(a), (b), and (c). The results for the outer surface of the upper plate suggest that the flow is completely attached to this surface except for $\alpha = 40°$ when the region of nearly uniform pressure downstream of $x_1 = 0{\cdot}3$ in. shows that separation is occurring near there. These conclusions were borne out by observations of a tufted rod.

Figures 17(a) and (c) also show that the pressures on the inner surfaces of the plates are nearly uniform for each value of α. They become increasingly more negative as α is increased until $\alpha = 40°$, when separation from the outer surface of the upper plate has occurred.

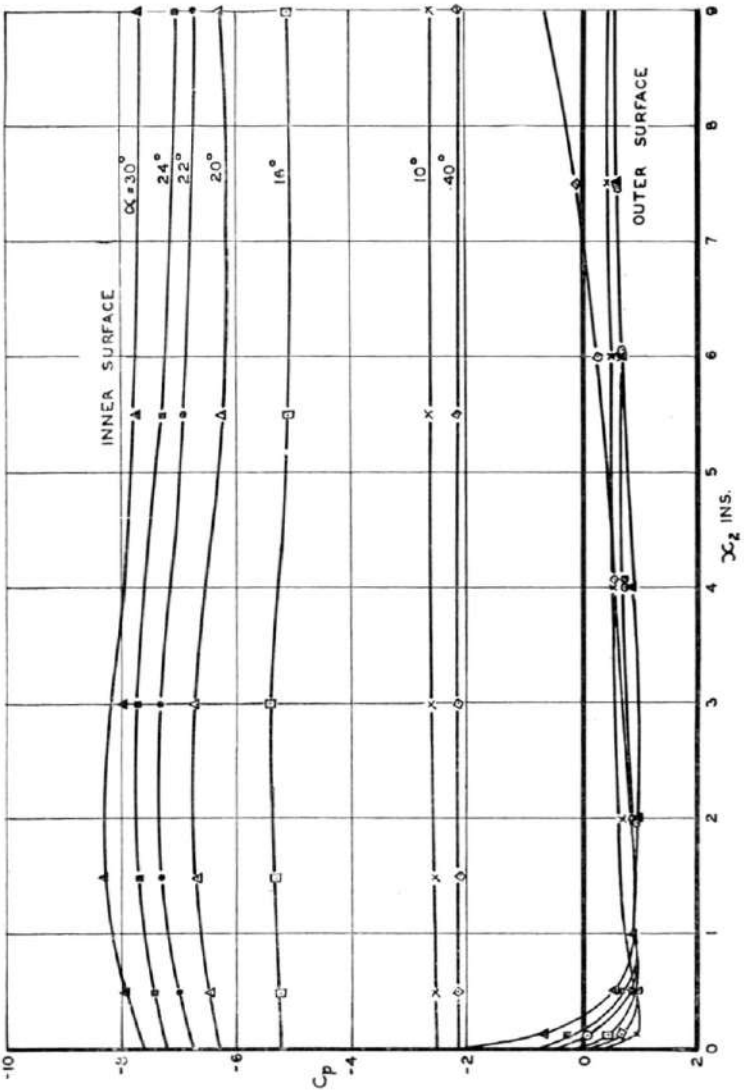

FIG. 17(a). Pressure distributions on lower plate for $C_\mu = 0{\cdot}46$, $\gamma = 130°$, and $\tau = 30°$.

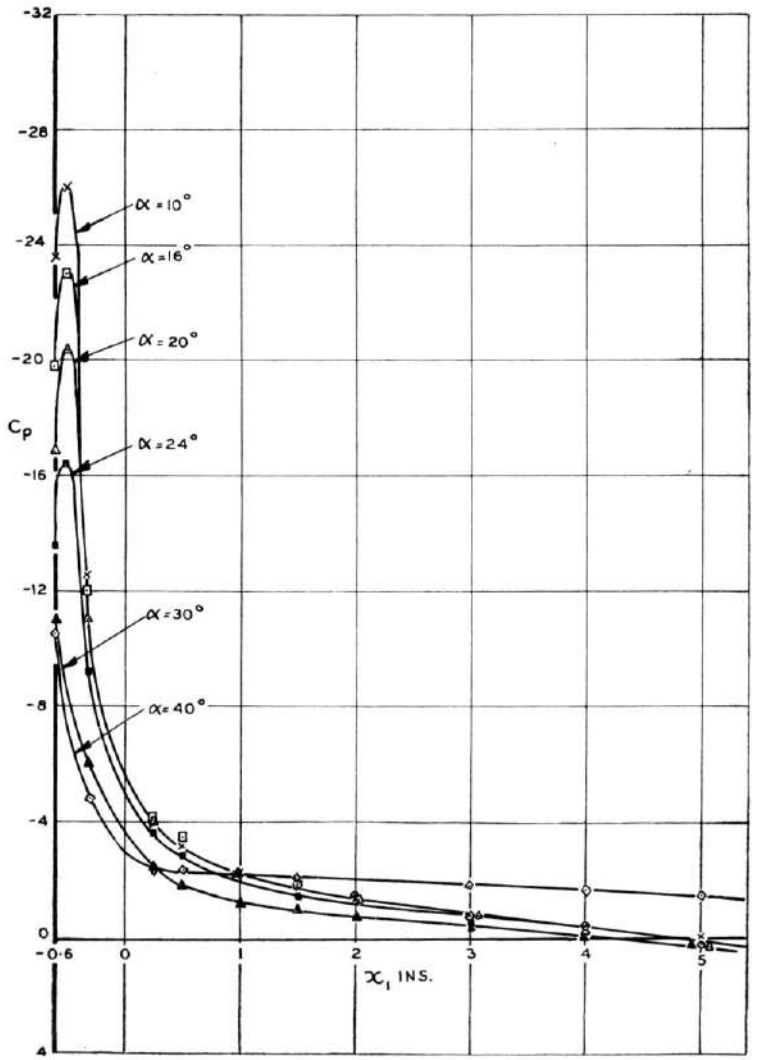

FIG. 17(b). Pressure distributions on outer surface of upper plate for $C_\mu = 0{\cdot}46$, $\gamma = 130°$, and $\tau = 30°$.

It is therefore concluded that it is possible to establish a free stream-line type flow for a range of values of α and not only for $\alpha = 22°$ as the potential theory might lead one to believe. The reason for this may be that the leading edge of the upper plate is rounded so that the reattaching flow can

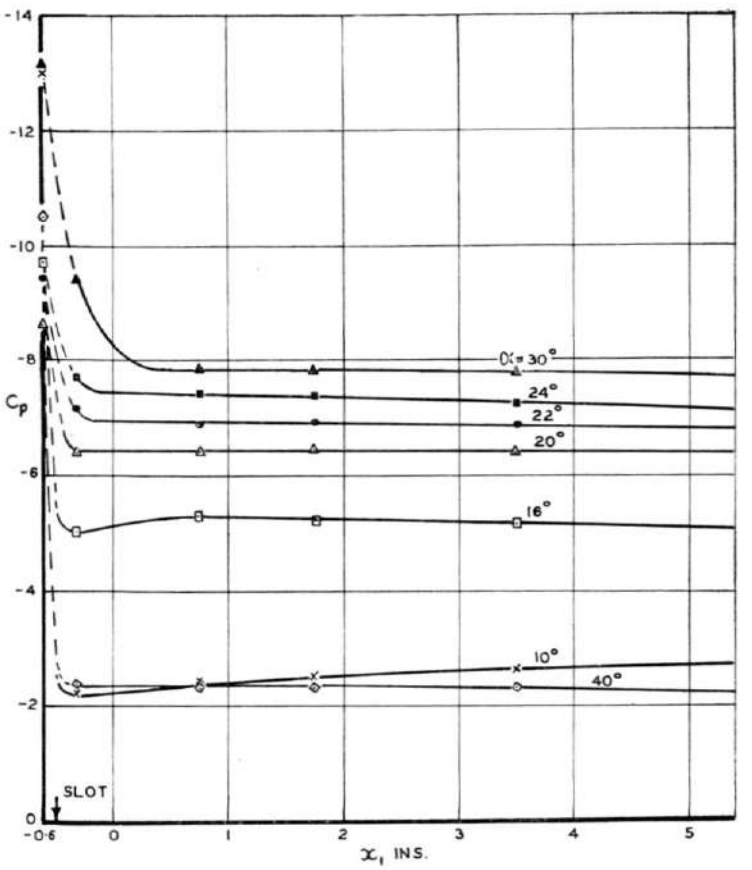

FIG. 17(c). Pressure distributions on inner surface of upper plate for $C_\mu = 0{\cdot}46$, $\gamma = 130°$ and $\tau = 30°$.

approach it in a number of directions and not only in the direction of the tangent to the upper plate as required by the theory. Evidence in support of this is provided by the flow visualization studies which are discussed immediately below.

Flow Visualization Studies. The results of the liquid film flow visualization studies are given in Fig. 18. A photograph of one of the patterns is given with its interpretation and also the interpretations of two other patterns. This work was done for $\gamma = 90°$ but it is appropriate to discuss it here where the general features of the flow are being considered.

Each pattern shows that there is a dividing stream line which separates

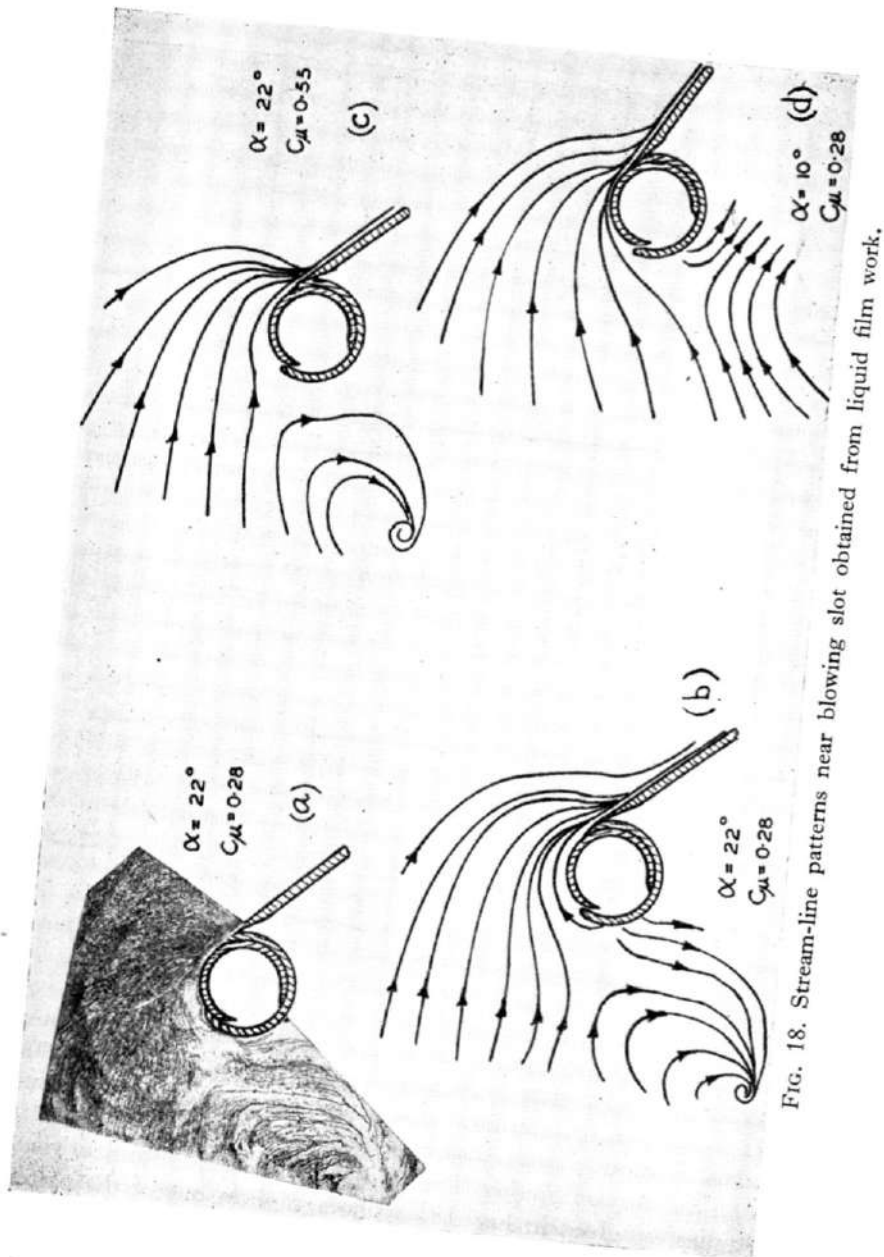

FIG. 18. Stream-line patterns near blowing slot obtained from liquid film work.

the flow which passes above the upper plate from the flow which circulates in the space between the plates.

Comparison of Figs. 18(b) and (d) shows the effect of changing α whilst keeping C_μ fixed. It is seen that when $\alpha = 22°$ the dividing stream-line approaches the blowing tube nearly in the direction of the free stream whereas when $\alpha = 10°$ its approach is inclined upwards.

Comparison of Figs. 18(b) and (c) shows the effect of changing C_μ whilst keeping α fixed. It is seen that for the larger value of C_μ the dividing stream-line is slightly higher and that the entrainment effect is larger.

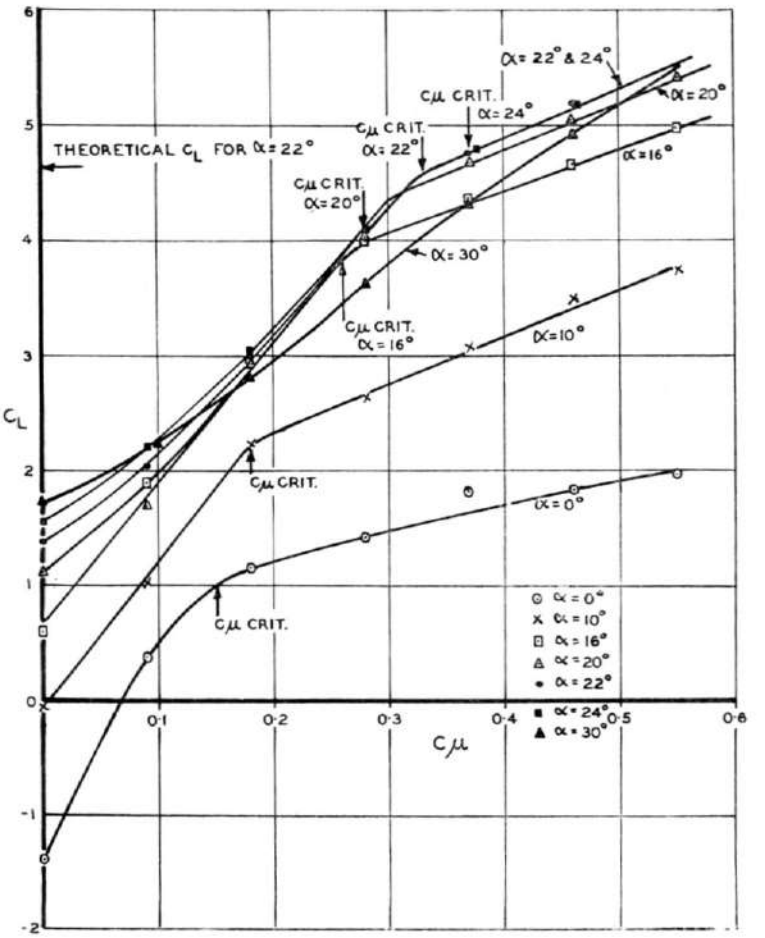

FIG. 19. $C_L - C_\mu$ curves for $\gamma = 130°$ and $\tau = 30°$.

Values of C_L. The $C_L - C_\mu$ curves for constant values of α are shown in Fig. 19. A noticeable feature of the curves is that C_L increases rapidly with C_μ up to a certain value of C_μ and that thereafter the increase is slower.

When conventional blowing over trailing edge flaps is employed the $C_L - C_\mu$ curves have the same feature and a typical set of results for this case is shown by the middle curve of Fig. 36. The explanation of this is well known. C_L increases rapidly with C_μ until the flow is completely attached to the upper surface of the flap and thereafter it increases slowly with C_μ due to the formation of a jet flap.

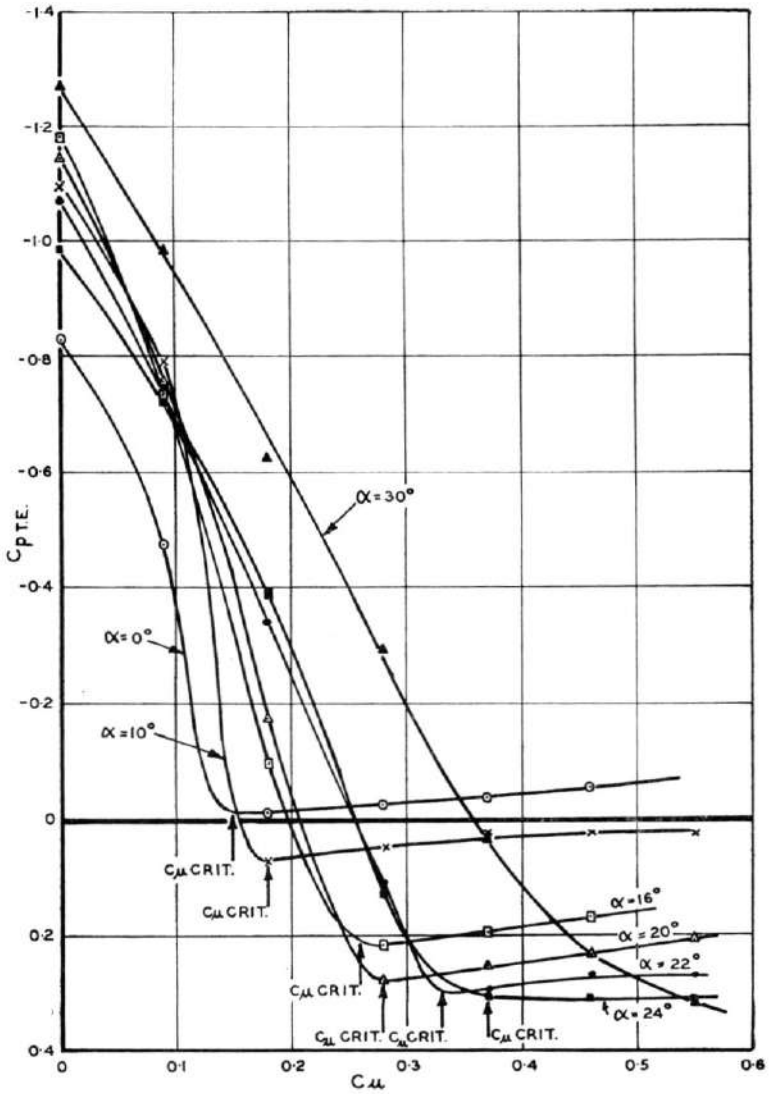

FIG. 20. Variation of *T.E.* pressure with C_μ for $\gamma = 130°$ and $\tau = 30°$.

To investigate if a similar explanation applied to the present tests the pressures measured at the hole on the upper surface of the upper plate closest to the trailing edge (0·4 in. upstream of it) were plotted as shown

in Fig. 20. It is known[5] that the trailing edge pressure is often a very sensitive indication of the existence of separation and the results of Fig. 20 show that this is so for the present tests. For each value of α, $C_{p.T.E.}$ increases rapidly with C_μ up to a certain value of C_μ and thereafter it remains nearly constant. The explanation is that as the extent of separated flow upstream of the trailing edge is reduced, both the pressure recovery upstream of the trailing edge and the pressure at the trailing edge increase. When the separation is completely suppressed the trailing edge pressure varies little with C_μ. The value of C_μ which is just sufficient to establish fully attached flow is thus the value that corresponds to the abrupt change in slope of the curve. This value is denoted by $C_{\mu\text{crit.}}$ The values of $C_{\mu\text{crit}}$ for the various values of α are indicated in Fig. 19 and it is seen that they correlate reasonably well with the changes in slope of the lift curves. It is therefore evident that this change occurs when the flow becomes fully attached to the upper plate.

The theoretical value of C_L when $\alpha = 22°$ is shown in Fig. 19 and it is seen that it agrees well with the measured value when $C_\mu = C_{\mu\text{crit.}}$

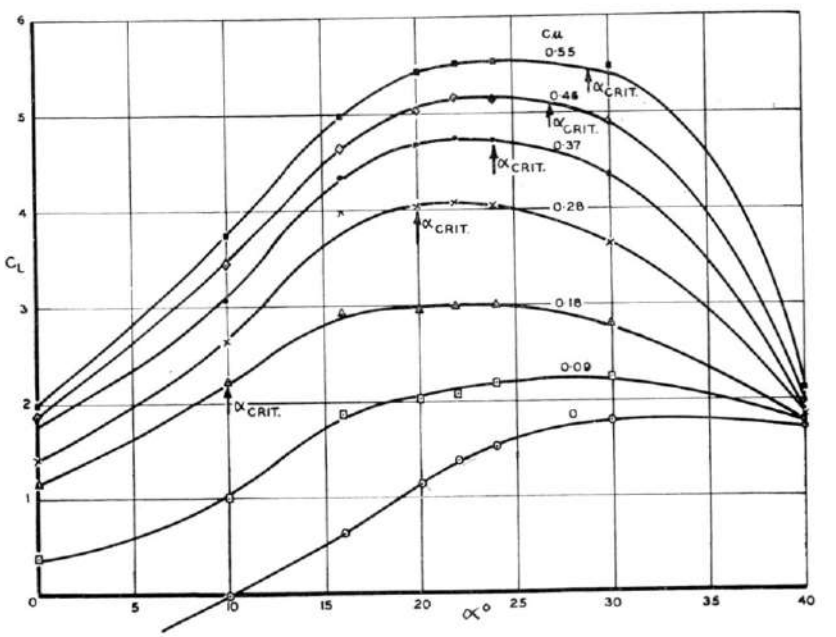

FIG. 21. C_L — α curves for $\gamma = 130°$ and $\tau = 30°$.

The C_L results are plotted against α for constant values of C_μ in Fig. 21. The values of α_{crit} shown were obtained by plotting $C_{\mu\text{crit}}$ against α (Fig. 22) and then reading off the values of α_{crit} for various values of $C\mu$. Thus for a given value of C_μ the flow will be attached to the whole of the outer surface of the upper plate for $\alpha < \alpha_{\text{crit}}$ but not for $\alpha > \alpha_{\text{crit}}$.

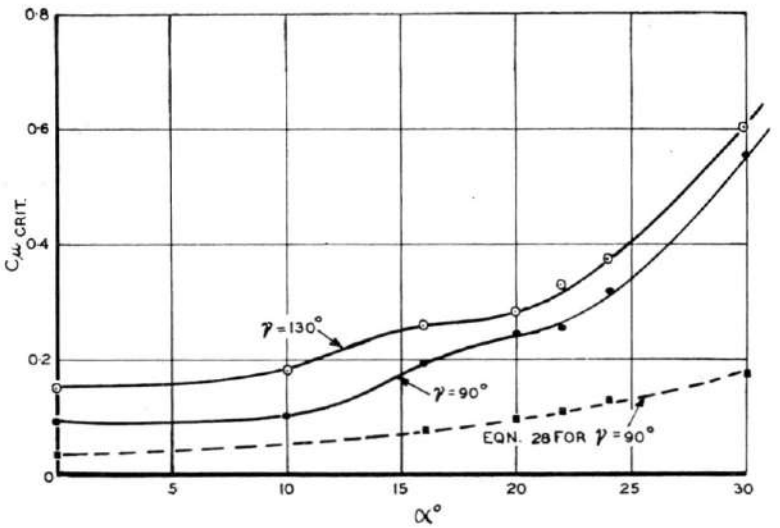

FIG. 22. Values of C_μ needed for complete attachment of flow to the outer surface of the upper plate.

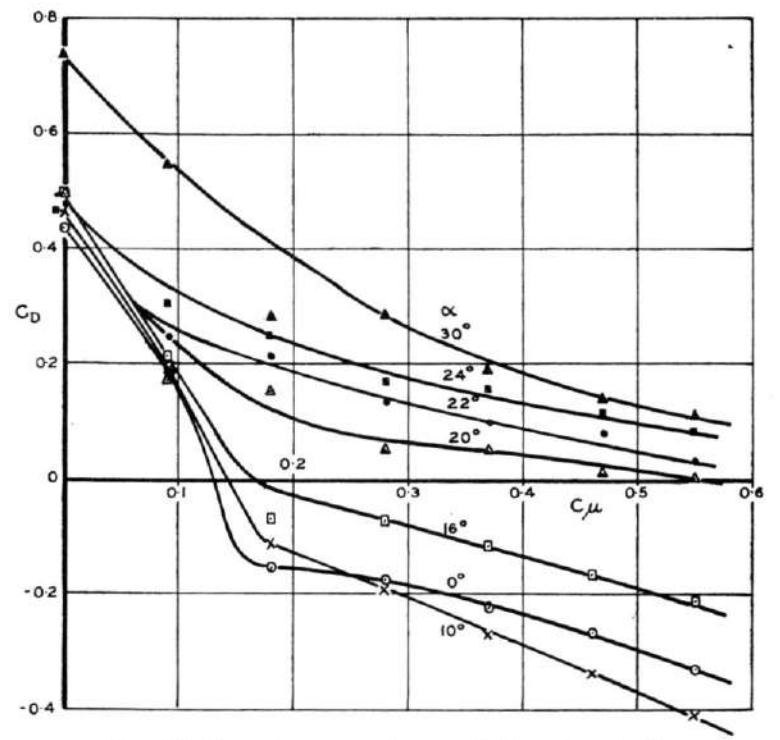

FIG. 23. $C_D - C_\mu$ curves for $\gamma = 130°$ and $\tau = 30°$.

The discussion of Fig. 21 is difficult because unlike a conventional aerofoil the "free stream-line aerofoil" changes its shape as the incidence is changed (see for example Fig. 18). However, a feature of the curves for which $C_\mu \geqslant 0{\cdot}28$ is that their slopes decrease very considerably before $\alpha = \alpha_{crit}$, i.e. before the flow has started to separate from the upper plate. It appears that the value of α at which the curves have zero slope is close to the theoretical value of 22°. The reason for this is not understood.

Values of C_D. The values of the form drag coefficient C_D are shown in Fig. 23 and it is seen that for small values of α and large values of C_μ, C_D is negative. This arises from the thrust that is produced by the sheet of high velocity air that leaves the trailing edge of the aerofoil. In discussing the drag results it is therefore convenient to consider the values of $C_{DT} = C_D + C_\mu$, which is a measure of the total drag associated with the wing flap arrangement, with the exception of the skin friction drag. C_{DT} includes the loss of thrust involved by discharging air out of the blowing slot rather than out of the tail pipe of the aeroplane with 100% efficiency

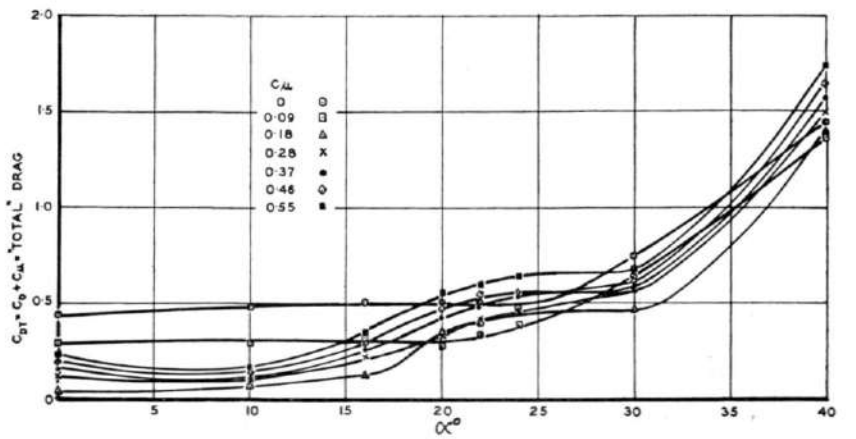

FIG. 24. C_{DT} — α curves for $\gamma = 130°$ and $\tau = 30°$.

The values of C_{DT} are given in Fig. 24 and the values of C_{DT}/C_L in Fig. 25. It is instructive to compare the latter results with the corresponding ones for a flat plate with completely separated flow on its upper surface. For this case the resultant force, N, on the plate is approximately in the direction of the normal to the plate so that

$$L = N \cos \alpha$$

$$D = N \sin \alpha$$

and

$$\frac{C_D}{C_L} = \tan \alpha$$

The values of tan α are included in Fig. 25 and it is seen that for the larger values of C_μ the present tests give much smaller values of the ratio of drag to lift. The reason is that without the flap the mixing region that

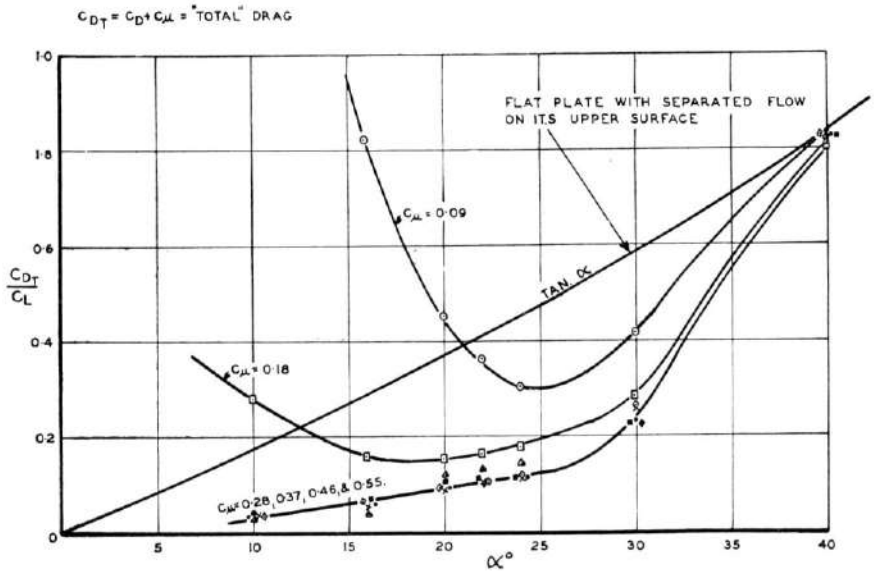

FIG. 25. Ratios of drag to lift and comparison with results for a flat plate with separated flow on its upper surface.

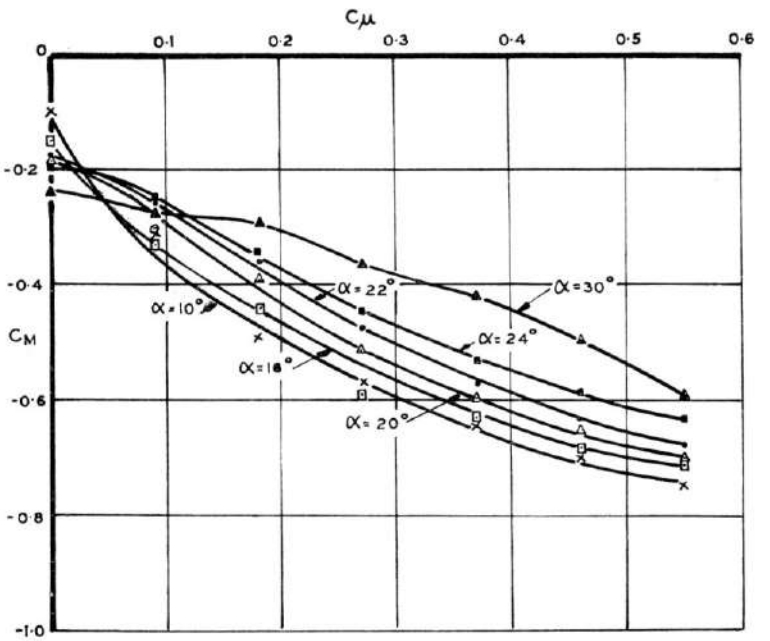

FIG. 26. $C_M - C_\mu$ curves for $\gamma = 130°$ and $\tau = 30°$.

originates at the leading edge of the plate extends well beyond the trailing edge of the plate so that the mixing losses are very large. When the flap is present the mixing region only extends to its leading edge so that the losses are much less. It is noted that the drag–lift ratio comparison would be even more favourable if it were made on a C_L rather than an α basis. This is because for a given α, C_L is much larger when the flap is present.

It is thus seen that the flap provides a mechanism for restoring a large portion of the leading edge suction which is normally lost when the flow separates from the leading edge of a wing.

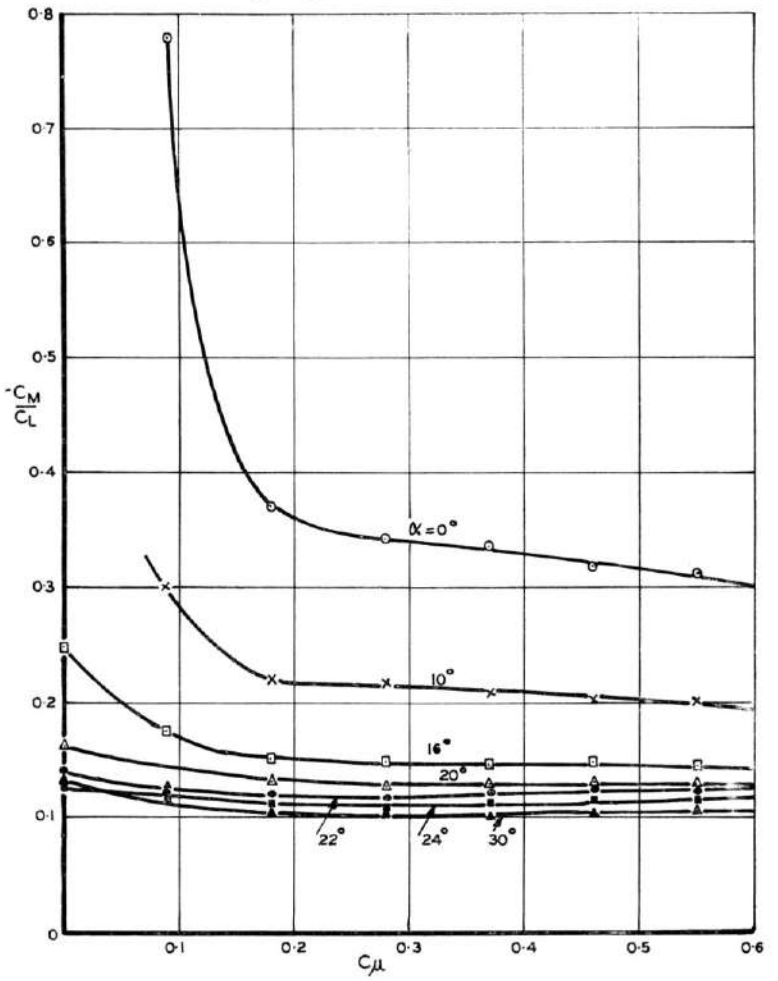

FIG. 27. $-C_M/C_L - C_\mu$ curves for $\gamma = 130°$ and $\tau = 30°$.

Values of C_M. The values of C_M are shown in Fig. 26, and Fig. 27 gives the values of $-C_M/C_L$. This quantity is approximately equal to $x_{C.P.}/C - 0{\cdot}25$ where $x_{C.P.}$ is the distance from the leading edge to the centre of

pressure. It is seen that $x_{C.P.}$ varies little with C_μ provided it is above a certain value. Also $x_{C.P.}$ decreases as α is increased.

In Fig. 28 a typical $C_M - C_L$ curve (that for $C_\mu = 0{\cdot}37$) is compared with the $C_M - C_L$ curve for an N.A.C.A. 23012 aerofoil fitted with a 30% chord double slotted flap which is deflected 40°[6]. It is seen that in each case the pitching moments are approximately the same.

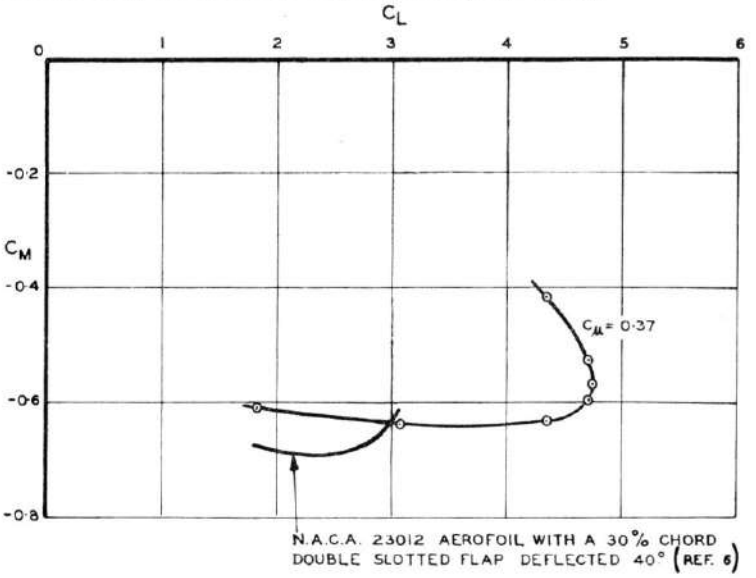

FIG. 28. Comparison of typical $C_M - C_\mu$ curve with that for the N.A.C.A. 23012 aerofoil fitted with a double-slotted flap.

Scale Effect

Pressure distributions were measured at wind-speeds of 35 ft/sec and 65 ft/sec to investigate scale effects. It was found that for equal values of C_μ the pressure distributions were very nearly independent of wind speed. The small scale effect indicated is not surprising since, according to mixing length theory, the mixing region which replaces the free stream-line is not influenced by changes in Reynolds number.

$\tau = 30°$, $\gamma = 90°$, and Various Values of α

Additional tests were carried out with the model in the same condition as for the previous tests with the exception that the slot angle γ was decreased from 130° to 90°.

For each value of α the complete pressure distributions were measured for only a small number of values of C_μ. The values of C_L were calculated from these results and a curve was constructed relating C_L with the pressure measured by one of the pressure tubes in the space between the plates. For the other values of C_μ, the C_Ls were obtained from the curve and measurements of this pressure.

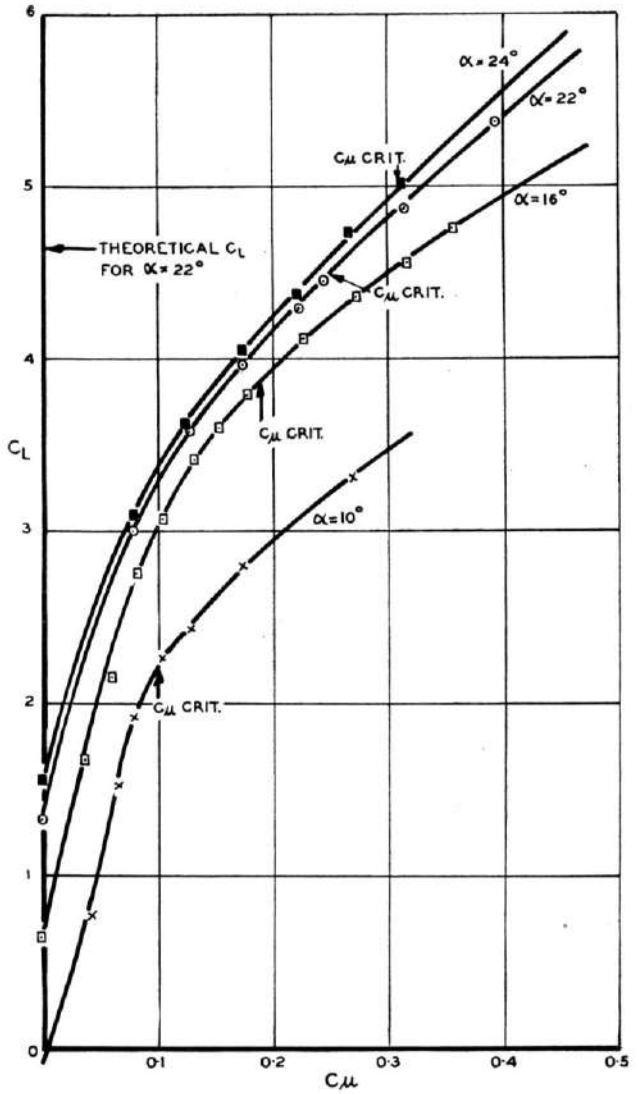

FIG. 29. $C_L - C_\mu$ curves for $\gamma = 90°$ and $\tau = 30°$.

Checks showed that this procedure gave accurate values of C_L. However, it was found that a similar procedure was not feasible for obtaining values of C_D and C_M so that no values of these quantities are given in this section.

Comparison of Figs. 29 and 19 shows that a smaller value of C_μ is needed to obtain a given C_L when $\gamma = 90°$ than when $\gamma = 130°$.

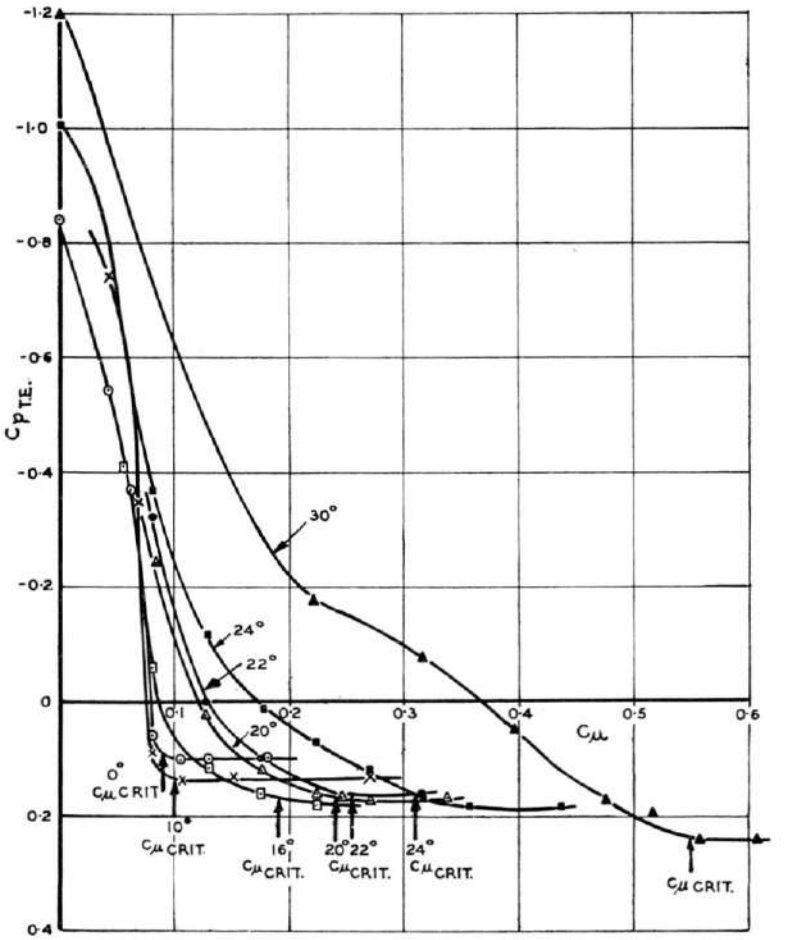

FIG. 30. Variation of *T.E.* pressure with C_μ for $\gamma = 90°$ and $\tau = 30°$.

Figure 30 gives the values of $C_{p.T.E.}$ and the values of $C_{\mu\text{crit}}$ (see p. 691) are indicated. It is seen that for the larger values of α, $C_{p.T.E.}$ approaches its nearly constant value much more slowly than when $\gamma = 130°$ (Fig. 20). Figures 29 and 19 show that this difference is reflected in the $C_L - C_\mu$ curves: the changes in slope are less abrupt when $\gamma = 90°$ than when $\gamma = 130°$.

Figure 29 shows that the measured value of C_L when $\alpha = 22°$ and $C_\mu = C_{\mu\text{crit}}$ is nearly equal to the theoretical value.

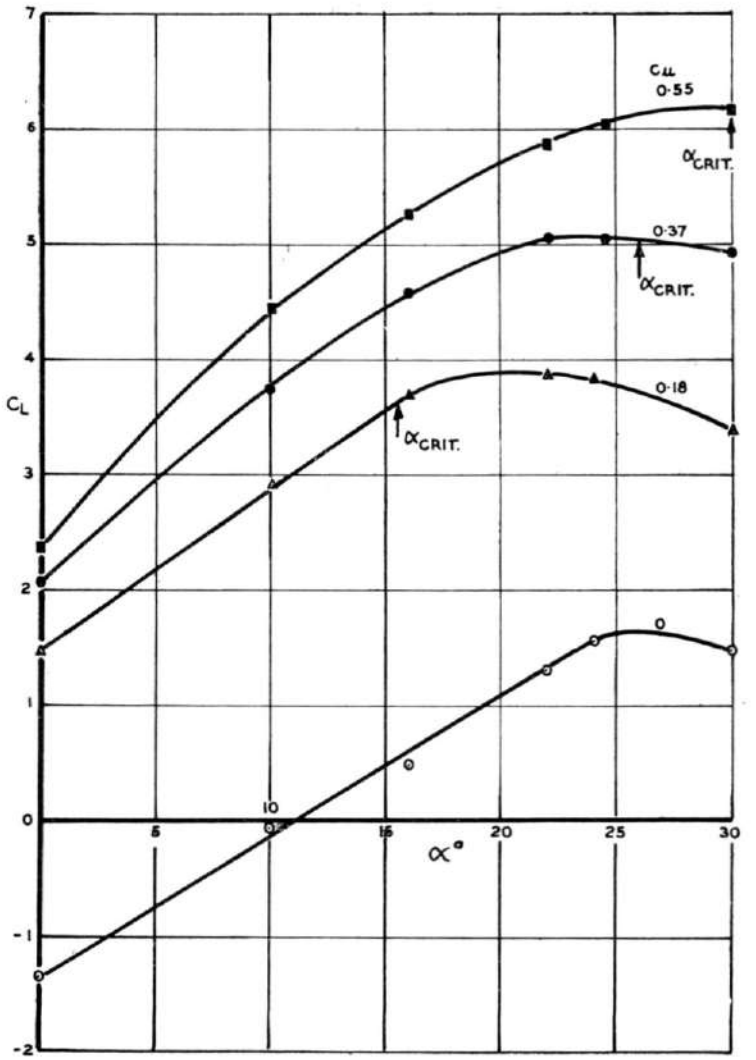

FIG. 31. $C_L - \alpha$ curves for $\gamma = 90°$ and $\tau = 30°$.

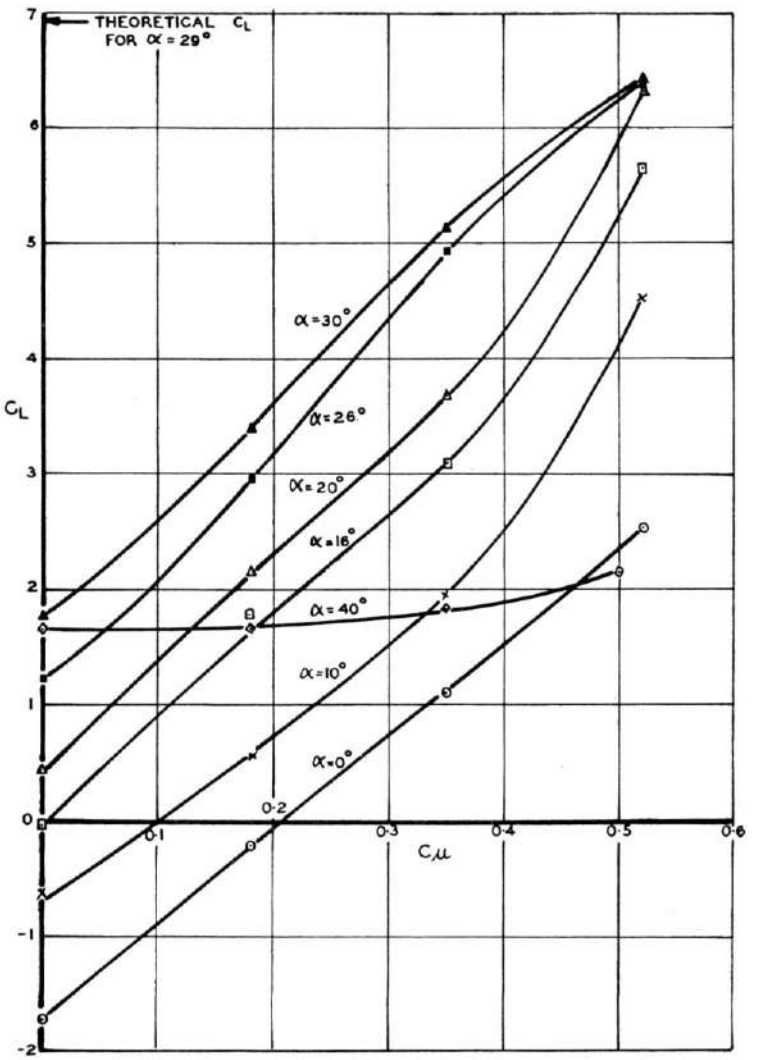

FIG. 32. $C_L - C_\mu$ curves for $\gamma = 130°$ and $\tau = 45°$.

Figure 31 shows that for $C_\mu = 0{\cdot}37$ and $0{\cdot}55$ the slopes of the $C_L - \alpha$ curves decrease markedly before $\alpha = \alpha_{crit}$ as was noted when $\gamma = 130°$ (see p. 693).

$\tau = 45°$, $\gamma = 130°$, *and Various Values of* α

Only a small number of measurements was made for this case and the lift results only, which are shown in Figs. 32 and 33, will be considered.

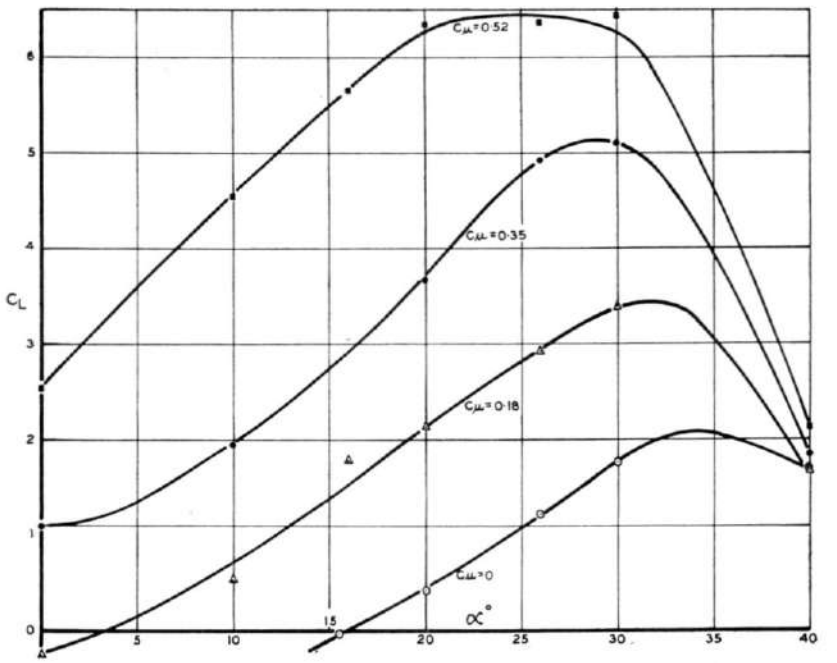

FIG. 33. $C_L - \alpha$ curves for $\gamma = 130°$ and $\tau = 45°$.

None of the $C_L - C_\mu$ curves of Fig. 32 shows the change in slope which has been shown to be indicative of the attainment of fully attached flow on the outer surface of the upper plate. It is concluded that in no case was the value of C_μ large enough.

The theoretical solution occurs when $\alpha = 29°$ and then $C_L = 6{\cdot}9$ (see p. 672). Figures 32 and 33 show that this value of C_L was not attained in the experiments, although for $\alpha = 30°$ and $C_\mu = 0{\cdot}52$ the C_L was $6{\cdot}4$.

Investigation of the Audio Note Emitted by the Model

Throughout the experiments it was observed that a regular audio note was emitted by the model when the blowing slot was working. Figure 34 shows how the Strouhal number of the note, Nl_2/U, varies with C_μ for the case $\alpha = 22°$, $\gamma = 130°$, and $\tau = 30°$. Results for a number of wind speeds are given and it is seen that the frequency, N, varies with the wind

speed. This shows that the note is not produced by a mechanical resonance and suggests that its origin is purely aerodynamic.

The Strouhal number is large and this suggests that the scale of the phenomena that is responsible for the note is small. It seems most likely

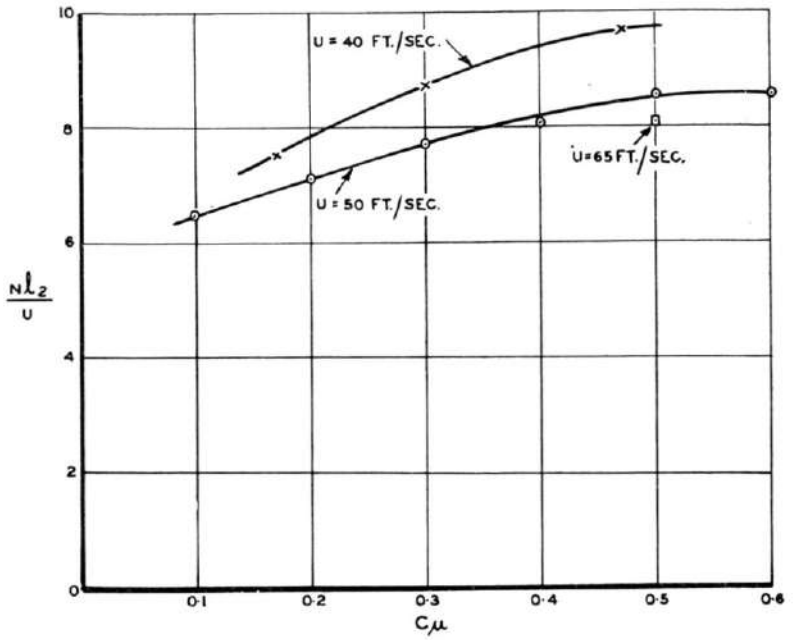

FIG. 34. Frequency of note emitted by model for $\alpha = 22°$, $\gamma = 130°$ and $\tau = 30°$.

that the note is produced by a small scale, high frequency, unsteadiness in the flow in the neighbourhood of the slot, although no such unsteadiness was detected.

8. THEORETICAL ESTIMATES OF THE VALUES OF C_μ NEEDED TO ESTABLISH FREE STREAM-LINE TYPE FLOWS

It was shown on p. 683 that the velocity profile in the mixing region at a distance s along the stream-line which separates from the leading edge of the lower plate is approximately the same as mixing length theory predictions of the velocity profile at a distance s downstream of the junction of a uniform stream with air at rest. This latter flow will be referred to as the analogous flow, the analogy between the flows being illustrated in Fig. 16.

Now by continuity considerations the stream-line which separates from the leading edge of the lower plate will divide where it meets the leading edge of the upper plate. The air flowing above it will pass down the upper

surface of the upper plate and the air flowing below it will circulate between the plates. In the analogous flow the corresponding stream-line is the one which originates at the lower edge of the uniform stream and is designated by $\psi = 0$ in Fig. 16. Thus if it is assumed that the mixing length analogy may be applied up to the leading edge of the upper plate it may be used to give an estimate of θ_R, the momentum thickness of the boundary layer just before it reattaches. For θ_R will be the momentum deficit of the air lying above the stream-line $\psi = 0$ at $s = L$, where L is the length of the free stream-line, so that

$$\theta_R = \int_{\psi=0}^{\psi=\infty} \frac{u}{U^*}\left(1 - \frac{u}{U^*}\right)\mathrm{d}y$$

the values of u/U^* being given by Tollmien's analysis. Thus it is found that

$$\theta_R = 0{\cdot}012L \tag{25}$$

It is interesting to compare θ_R with the value θ'_R that would occur at the same position if the free stream-line were replaced by a solid surface. If it is assumed that transition occurs at the leading edge in the latter case then the flow is the same as that along a flat plate so that[7]

$$\theta'_R = 0{\cdot}036L\left(\frac{\nu}{U^*L}\right)^{1/5} \tag{26}$$

Equations (25) and (26) show that as U^*L/ν increase from 10^4 to 10^7, θ'_R/θ_R decreases from 0·49 to 0·12.

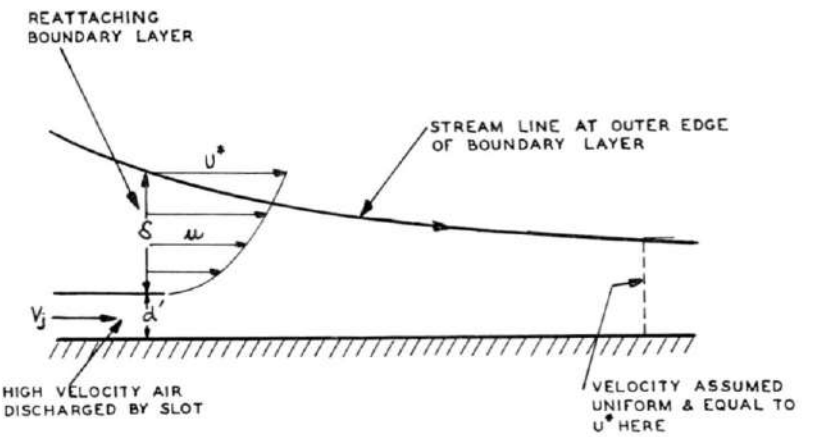

FIG. 35. Estimation of $C_{\mu R}$.

The effect on the reattaching boundary layer of the high velocity air discharged by the slot will now be considered. The process is idealized as shown in Fig. 35. It is assumed that the reattaching boundary layer, of momentum thickness, θ_R, mixes at pressure $C_p{}^*$ with the high velocity air that is discharged by the slot. Simple mixing theory is used to calculate

the value of C_μ, denoted by $C_{\mu R}$, that is needed to restore the average velocity in the boundary layer to U^*, the velocity outside the layer.

If it is assumed that the velocity in the boundary layer is uniform and equal to U^* at some downstream station then the application of the momentum theorem between this station and the upstream station shown in Fig. 35 gives

$$\int_0^\delta \rho u^2 \, dz + \rho V_j^2 d' = U^* \left(\rho V_j d' + \int_0^\delta \rho u \, dz \right)$$

so that

$$\int_0^\delta u(U^* - u) \, dz = V_j^2 d' - U^* V_j d'$$

Dividing by $U^2 l_2$ gives for $V_j \gg U^*$

$$\frac{U^{*2}}{U^2} \frac{\theta_R}{l_2} = \frac{V_j^2 d'}{U^2 l_2} = \frac{1}{2} C_{\mu R}$$

so that

$$\begin{aligned} C_{\mu R} &= \frac{2U^{*2}}{U^2} \frac{\theta_R}{l_2} \\ &= 2(1 - C_p^*) \frac{\theta_R}{l_2} \\ &= 0{\cdot}024(1 - C_p^*) \frac{L}{l_2}, \qquad \text{by equation (25)} \end{aligned} \tag{27}$$

where C_p^* is the pressure coefficient on the free stream-line.

Taking $L/l_2 = 0{\cdot}677$, the value given by the potential solution shown in Fig. 7 gives

$$C_{\mu R} = 0{\cdot}016(1 - C_p^*) \tag{28}$$

C_p^* will be approximately equal to the nearly uniform pressure coefficient in the space between the plates. The measured values of this coefficient when $\gamma = 90^\circ$ and $C_\mu = C_{\mu\,\text{crit}}$, the value of C_μ needed to establish the free stream-line type flow (see p. 691), were substituted into equation (28) to give values of $C_{\mu R}$. These values are shown in Fig. 22 and it is seen that they vary between a half and a third of the values of $C_{\mu\,\text{crit}}$. It is thus suggested that an approximate expression for $C_{\mu\,\text{crit}}$ is

$$C_{\mu\,\text{crit}} = 2{\cdot}5 C_{\mu R} = 0{\cdot}06(1 - C_p^*) \frac{L}{C}, \qquad \text{from equation (27)} \tag{29}$$

One check that can be made on this formula is to use it to estimate $C_{\mu\,\text{crit}}$ when $\tau = 45^\circ$ and $\alpha = 29^\circ$, when there is a potential solution (see p. 672). Then $q_m/U = 3{\cdot}1$ so that

$$1 - C_p^* = (3{\cdot}1)^2 = 9{\cdot}6$$

Taking $L/C = \frac{3}{2}$ times its value when $\tau = 30$ gives $L/C = 1{\cdot}0$, so that from equation (29)

$$C_{\mu\,\text{crit}} = 0{\cdot}58$$

Figure 32 shows that for $\alpha = 30°$ and $C_\mu = 0{\cdot}52$, C_L is 6·4, which is slightly below the theoretical value of 6·9. The estimate of $C_{\mu\,\mathrm{crit}}$ is thus reasonably close.

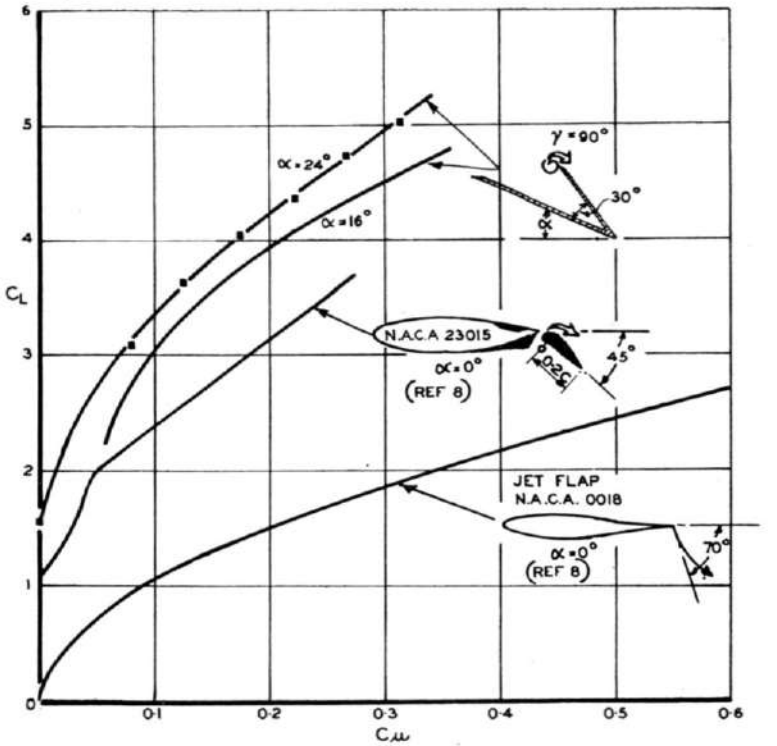

FIG. 36. Comparison of C_L values with those obtained by other methods.

9. COMPARISON OF C_L VALUES WITH THOSE OBTAINED BY OTHER METHODS

In Figure 36 two of the $C_L - C_\mu$ curves of Fig. 29 are compared with typical results[8] for the jet flap and for blowing over trailing edge flaps. The comparison shows that the present scheme compares favourably with both the others both as regards the values of C_L that are achieved and the values of C_μ that are needed. It should be pointed out, however, that the comparison would be less favourable if it were made for equal values of the incidence. This was not done as suitable results for the other schemes at large incidences were not available.

10. CONCLUDING REMARKS

It has been shown that if a forward facing flap having a single blowing slot in its leading edge is mounted above a wing having a sharp leading edge, then flows of the free stream-line type can be established. The flow separates from the leading edge of the wing and reattaches to the leading

edge of the flap. Large lifts are obtained for moderate blowing quantities (Fig. 36) and the total drag associated with the scheme is not large (Fig. 25).

As was remarked on p. 664 the wing-flap arrangement that was used for these initial tests was chosen because it was simple enough to enable calculations of the potential flow to be made. For practical applications other arrangements would be preferable.

For example it would appear to be advantageous to mount the flap ahead of the trailing edge of the aerofoil as shown in Fig. 1(b). Since the flap leads to a large increase in the chordwise loading only between the leading edge of the wing and the leading edge of the flap it should be possible to design this generalized arrangement so that the centre of pressure is near the quarter chord point. The lifts obtained would be smaller than in the present tests but on the other hand so would the values of C_μ that would be needed.

The circular duct that was used to feed the blowing slot may not be suitable for practical applications as it might be too thick to retract into a thin wing. An oval duct would probably be required and this would lead to the flap having a more curved leading edge. Tests on such an arrangement are needed.

A model is being constructed to investigate the three-dimensional effects that arise when the flap is mounted on an unswept wing of finite aspect ratio.

It is possible that a forward facing flap could be used to increase the lift and decrease the drag of a thin slender delta. At other than small incidences the flow separates from the leading edge and a pair of symmetrically placed conical vortices are formed. In this case the flap would be such as to preserve the conical nature of the flow and a possible arrangement on which boundary layer control may not be needed is shown in

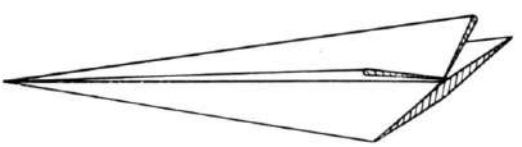

FIG. 37. Forward facing flap mounted on thin slender delta

Fig. 37. In this case the pressure would not be constant along the streamline which separated from the leading edge of the wing and a different stream-line would reattach to the leading edge of the flap.

Acknowledgements. The author wishes to acknowledge his great indebtedness to Mr. N. Ruglen who carried out most of the experimental work, and to Mr. P. R. Skeat for the numerical calculations.

He also wishes to thank the Chief Scientist, Department of Supply, for permission to give this paper.

REFERENCES

1. D. G. Hurley and P. R. Skeat, A Series of Aerofoils Designed to Develop Exceptionally Large Lift Coefficients when Boundary Layer Control by Blowing is Employed, Report A.R.L./A.102, March 1957.
2. D. G. Hurley and N. Ruglen, The Use of Boundary Layer Control to Establish Free Stream-Line Flows being an Introduction to the Free Stream-Line Flap, Report A.R.L./A.109, April 1958.
3. J. Black, A Note on the Mixing Process in the Flow Induced by a High-Velocity Air-Jet, *J. Roy. Aero. Soc.*, Vol. 61, September 1957.
4. W. Tollmien, Calculation of Turbulent Expansion Processes, N.A.C.A. T.M. 1085.
5. H. H. Pearcey, Some Effects of Shock-Induced Separation of Turbulent Boundary Layers on Transonic Flow Past Aerofoils. Paper delivered at Symposium on Boundary Layer Effects in Aerodynamics, N.P.I., England, March 1955.
6. Abbott and von Doenhoff, *Theory of Wing Sections*. McGraw-Hill, New York, p. 219.
7. S. Goldstein (Editor), *Modern Developments in Fluid Mechanics*, pp. 361–2.
8. P. Poisson-Quinton, Quelques Aspects Physiques du soufflage sur les ailes d'avion. *Tech. Sci. Aero.* Vol. 4, 1956.

DISCUSSION

R. C. Pankhurst†: Mr. Hurley is to be congratulated on the investigations described in his paper. The concept of the free stream-line flap is a novel one, and perhaps few of us would have been brave enough to subject it to the test of experimental verification. Usually boundary-layer control is regarded merely as a means of increasing lift or reducing drag, but the free stream-line flap provides an interesting example of its use to establish a different type of flow pattern which probably could not have been set up at all without it.

In the past, attempts to set up unorthodox types of flow have sometimes produced unexpected flow unsteadiness or flow instability. Were any such effects encountered with the free stream-line flap?

A second question is prompted by the necessarily low Reynolds numbers of the small-scale experiments described in the paper: what sort of scale effect is to be expected?

Thirdly (although this question, too, may be somewhat premature at present) what are the probable effects of finite aspect ratio?

D. G. Hurley: I would like to thank Dr. Pankhurst for his remarks and to add that we were pleasantly surprised when we found that we could establish the type of flow we wanted.

As regards flow unsteadiness, tufted rod investigations indicated that the flow outside the mixing region was perfectly steady. However, throughout the course of the experiments the model emitted a regular audio note except when the blowing air was turned off. Its Strouhal number was approximately 8 (see Fig. 34) which suggests that it is associated with a small-scale unsteadiness which probably occurs near the reattachment point. Attempts to confirm this using smoke and a stroboscope were not successful.

† Aerodynamics Division, National Physical Laboratory, England.

Scale effects were investigated for Reynolds numbers between $1{\cdot}46 \times 10^5$ and $3{\cdot}18 \times 10^5$. For a given value of C_μ the pressure distributions were found to be nearly independent of Reynolds number. This small scale effect was expected as according to mixing length theory the value of C_μ needed to establish the flow is independent of Reynolds number (see p. 702).

The effects of finite aspect ratio are to be investigated on a half model of an unswept wing of aspect ratio 8. It is anticipated that the flow will be quasi-two-dimensional except near the tip.